CURVED WALL BOUNDARY LAYER FLOW

K. R. L. Perera

United States
Naval Postgraduate School

THESIS

CURVED WALL BOUNDARY LAYER FLOW

by

K. R. L. Perera

Thesis Advisor: T. Houlihan

June 1971

Approved for public release; distribution unlimited.

Curved Wall Boundary Layer Flow

by

K. R. L. Perera
Lieutenant Commander, Royal Ceylon Navy
Royal Naval Engineering College, 1963

Submitted in partial fulfillment of the
requirements for the degree of

MASTER OF SCIENCE IN MECHANICAL ENGINEERING

from the

NAVAL POSTGRADUATE SCHOOL
June 1971

Thesis
P 3253
c.1

ABSTRACT

Mean velocities, turbulence intensities, and Reynolds stresses were measured in a circular convex wall jet. The entire mean velocity profile for angular position $\theta > 35$ degrees was determined to be similar. The turbulent flow field was nowhere self preserving and thus the total flow was not similar. Strikingly different jet growth rates were evidenced between the inlet ($\theta < 35$ degrees) transition region and the fully developed flow regions ($\theta > 35$ degrees). The overall level of turbulence was found to be higher for a convex wall jet flow in comparison to a concave wall jet flow. However, maximum turbulence intensities occurred closer to the wall for increasing distance along the surface indicating the stabilizing effect of the convex wall. The turbulent shear stress $\overline{u'v'}$ was dominant in comparison with $\overline{u'w'}$ and did not vanish where the mean velocity gradient became zero. Hence for further analyses of turbulent convex wall jet flow the classical eddy viscosity models which neglect the effects of curvature cannot be incorporated.

TABLE OF CONTENTS

LIST OF ILLUSTRATIONS

LIST OF SYMBOLS

A_c	cross sectional area of nozzle
b	representative jet thickness as defined in Eq. (7)
CF(P)	pressure correction factor
CF(T)	temperature correction factor
m, n, p	exponents as defined in Eqs. (7b) and (10)
P	pressure
P_t	total pressure
Re_w	Reynolds number based on width of nozzle
R	radius of curvature of quadrant
s	constant as defined in Eq. (7b)
u, v, w	local mean velocity components
u', v', w'	turbulent velocity components (rms values)
U_m	maximum fluid velocity in a given profile
$U_{m/2}$	one half of maximum fluid velocity
U_o	average velocity in the nozzle
W	power jet width
X, k	constants as defined in Eq. (7)
x	downstream distance measured from origin of jet
y	distance from surface to the local velocity
y_m	distance from surface to the maximum local velocity
$y_{\frac{m}{2}}$	distance from surface to point where $u = 0.5\ U_m$
Θ	convex wall angular position
ν	kinematic viscosity
μ	dynamic viscosity
ρ	fluid density
τ	shear stress
ψ	stream function
δ	boundary layer thickness

η	dimensionless coordinate
$f(\eta)$	dimensionless stream function
$g_1(\eta), g_2(\eta), g_{12}(\eta)$	dimensionless parameters as defined in Eq. (10)

ACKNOWLEDGEMENT

The author wishes to express his appreciation to Professor T. Houlihan for his guidance and advice during the course of the investigation. A special note of appreciation is also extended to Messrs. K. Mothersell and J. McKay, of the Mechanical Engineering Machine Shop, for their assistance in setting up the experimental apparatus.

I. INTRODUCTION

The need for a basic understanding of the flow field common to fluid computing elements underlies a series of investigations at the Naval Postgraduate School involving two dimensional wall jets blowing over both plane and curved surfaces.

Extensive studies were undertaken by Kesler [1] and Johnson [2] on the attachment of turbulent wall jets to convex walls. The effects of both wall setback and control port opening on such flows were fully investigated in these studies. Richardson [3] extensively investigated the flow in a two dimensional inclined plane wall jet which again contained both a control port and a setback. These studies supplement the investigations involving wall jets flowing over plane and curved surfaces previously performed by Sawyer [4], Newman [5], Fekete [6] and Guitton [7].

The classical theoretical study of the plane "wall jet" is that of Glauert [8], who designated the flow field as such. More recently Wyganski and Champagne [9] considered the laminar flow over a curved surface and determined a unique similarity condition for this configuration.

Schwarz and Cosart [10] determined that the flow in an incompressible, turbulent, plane wall jet configuration was self preserving. This self preservation was primarily based upon the assumption that the laminar viscous stresses were negligibly small in comparison to the turbulent Reynolds stresses of the flow.

Giles, Hays and Sawyer [11], by considering the equations of motion, again with the viscous terms neglected, proved that the flow in the outer part of a two dimensional, curved, turbulent wall jet blowing over a surface of a logarithmic spiral profile is self preserving.

Finally, Margolis and Lumley [12] performed a detailed study of turbulence in curved layers in a closed channel. This investigation

showed that for a convex surface (the "unstable" case) the curved shear layer spreads more rapidly than for a concave surface. By considering turbulent energy balance these investigators concluded that turbulent transport increased rapidly, as the flow developed, in the unstable case and decreased in the stable case (concave surface).

Considering the foregoing, an investigation of the flow field in a curved wall jet wherein both the laminar and the turbulent stresses are considered is recognized as a configuration needing investigation.

Thus, the experimental portion of the present study is a comprehensive investigation of the flow field of a two dimensional, turbulent wall jet over a convex surface of constant radius. There is no control port or setback on the test section.

The theoretical portion defines two attempts to determine a similarity condition for the flow by the introduction of a suitable eddy viscosity formulation into the flow equations. Neither attempt resulted in a successful conclusion.

II. THEORETICAL CONSIDERATIONS

The equations of motion and continuity for a two dimensional, incompressible and turbulent flow over a curved wall may be written 13, p. 112 4th ed. , neglecting terms in the order of $(y_m/R)^2$ and higher, as

$$u\frac{\partial u}{\partial x} + (1+y/R)v\frac{\partial u}{\partial y} + \frac{uv}{R} = -\frac{1}{\rho}\frac{\partial}{\partial x}\left(P+\rho\overline{u'^2}\right)$$

$$-(1+y/R)\frac{\partial}{\partial y}(\overline{u'v'}) - \frac{2}{R}\overline{u'v'} + \nu\left[(1+y/R)\frac{\partial^2 u}{\partial y^2} + \frac{1}{R}\frac{\partial u}{\partial y}\right] \qquad (1)$$

$$\frac{u^2}{R} = (1+y/R)\frac{1}{\rho}\frac{\partial}{\partial y}\left(P+\rho\overline{v'^2}\right) \qquad (2)$$

$$\frac{\partial u}{\partial x} + \frac{\partial}{\partial y}\left[(1+y/R)v\right] = 0 \qquad (3)$$

The total shear stress, that is viscous and turbulent, may be written as

$$\tau = \mu(1+y/R)\frac{\partial}{\partial y}\left(\frac{u}{1+y/R}\right) - \rho\overline{u'v'} \qquad (4)$$

Introducing Eq. (4) into Eq. (1) and simplifying, one has, for isotropic turbulence,

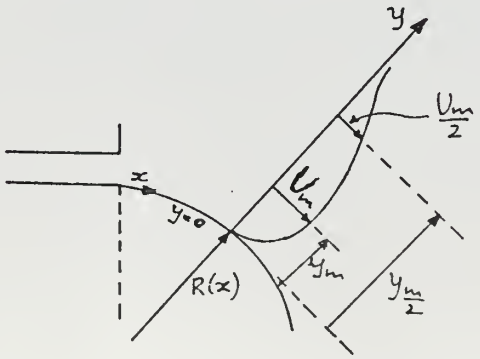

$$U\frac{\partial U}{\partial x} + (1 + y/R)V\frac{\partial U}{\partial y} + \frac{UV}{R} = -\frac{1}{\rho}\frac{\partial}{\partial x}\left(P + \rho\overline{v'^2}\right)$$

$$+ \frac{1}{\rho}\left[(1 + y/R)\frac{\partial \tau}{\partial y} + \frac{2}{R}\tau\right] \tag{5}$$

Integrating Eq. (5) from $y \to \infty$ and evaluating terms leads to the following general form [3 Eq. (20) p. 25]

$$\frac{d}{dx}\int_0^\infty U(1 + y/R)\left\{\int_y^\infty \frac{U^2}{1 + y/R}\,dy\right\}dy = \int_0^\infty (1 + y/R)V\left\{\int_y^\infty \frac{U^2}{R(1 + y/R)}\,dy\right\}dy$$

$$- \frac{1}{R}\int_0^\infty U\left\{\int_y^\infty UV\,dy\right\}dy - \frac{1}{\rho}\int_0^\infty (1 + y/R)U\tau\,dy + \frac{1}{\rho R}\int_0^\infty U\left\{\int_y^\infty \tau\,dy\right\}dy \tag{6}$$

Wyganski [9], using an analogous procedure to that used by Glauert [8], in which the latter derived an integral invariant by considering the exterior momentum flux, obtained a unique similarity solution for both convex and concave surfaces when the local radius of curvature is proportional to $x^{3/4}$.

In an analogous manner, a search was made for a similarity stream function for Eq. (5), using the turbulent shear model employed by Sawyer [11],

$$\tau = X b U_m\left(\frac{\partial U}{\partial y} - k\frac{U}{R}\right) \tag{7}$$

where X and k are constants and b(x) and $U_m(x)$ are the jet thickness and local maximum velocity. The boundary conditions for the flow of a jet over a surface are

$$\begin{aligned} &y = 0,\ u = v = 0 \\ &y \to \infty,\ u = 0 \end{aligned} \tag{7a}$$

Defining a similarity stream function as $u = \frac{\partial \psi}{\partial y}$, $(1+y/R)v = -\frac{\partial \psi}{\partial x}$ where $\psi = x^m f(\eta), \eta = sy/x^n$ and the radius of curvature $R = \alpha x^p$ (7b)

and substituting from above in Eq. (5) one obtains

$$x^{2m-2n-1}\left[s(m-n)(f')^2 - sn\eta f'f'' + s(n\eta f' - mf)f'' + \frac{1}{\alpha(1+\eta/s\alpha)}(n\eta f' - mf)f' + s\int_\eta^\infty \frac{\{2(m-n)(f')^2 - 2n\eta f'f''\}}{\alpha(1+\eta/s\alpha)} d\eta\right]$$

$$- x^{m-3n}\left[sbU_m X\left\{(1+\eta/s\alpha)(sf''' - \frac{k}{\alpha}f'') + \frac{2}{\alpha}(f'' - \frac{k}{s\alpha}f')\right\}\right] = 0 \quad (8)$$

For similar solutions to exist the equation should become independent of x, which leads to the requirement that

$$m + n = 1 \quad (9)$$

To obtain a second relation between m and n attempts were made to derive an integral invariant by considering the exterior momentum flux, as in the studies of Glauert [8] and Wygnanski [9]. An invariant condition exists if the right hand side of Eq. (6), with the shear stress as in Eq. (7) and for the given boundary conditions, could be proved to be equal to zero. Three approaches used in attempts at proving this condition ultimately failed.

In a further attempt, following Schwarz and Cosart, similarity functions were defined such that

$$u = U_m f(\eta), \quad \overline{u'^2} = U_m^2 g_1(\eta), \quad \overline{v'^2} = U_m^2 g_2(\eta), \quad \overline{u'v'} = U_m^2 g_{12}(\eta), \quad \eta = y/\delta \quad (10)$$

In Eq. (1) and (2) writing, for isotropic turbulence,

$(P + \overline{\rho u'^2}) = (P + \overline{\rho y'^2}) = P_t$ and eliminating P_t in Eq. (1) and (2) the following equation is obtained,

$$\frac{\partial U}{\partial y}\left[U\frac{\partial U}{\partial x} - \left\{\int_0^\eta \frac{\partial U}{\partial x}\,dy\right\}\frac{\partial U}{\partial y} - \frac{\nu}{R} - \frac{2}{R(1+y/R)}\left\{\int_0^\eta \frac{\partial U}{\partial x}\,dy\right\}\right]$$
$$+ \frac{U}{R}\left\{-\frac{1}{(1+y/R)}\left(\frac{\partial U}{\partial x} + \frac{\nu}{R}\right)\right\} + \frac{2(R+y)U\frac{\partial U}{\partial x} - U^2\frac{\partial R}{\partial x}}{(R+y)^2} \tag{11}$$
$$= -\left(1 + y/R\right)\frac{\partial^2 \overline{u'v'}}{\partial y^2} - \frac{3}{R}\frac{\partial \overline{u'v'}}{\partial y}$$

Substituting in Eq. (11) from (10) the following form is obtained after suitable rearrangement,

$$\frac{U_m^3}{\delta^2}\frac{\partial \delta}{\partial x}(f')^2\int_0^\eta \eta f'\,d\eta - \frac{U_m^2}{\delta}\frac{\partial U_m}{\partial x}(f')^2\int_0^\eta f\,d\eta + \frac{U_m^2}{\delta}\frac{\partial \delta}{\partial x}\frac{f'\int_0^\eta \eta f'\,d\eta}{R(1+\eta\delta/R)}$$
$$- U_m\frac{\partial U_m}{\partial x}\frac{f'}{R(1+\eta\delta/R)}\int_0^\eta f\,d\eta + \frac{U_m^2}{\delta}\frac{\partial \delta}{\partial x}\frac{f\eta f'}{R(1+\eta\delta/R)} - U_m\frac{\partial U_m}{\partial x}\frac{f^2}{R(1+\eta\delta/R)} \tag{12}$$
$$+ U_m^2\frac{\partial \delta}{\partial x}\frac{f}{R^2(1+\eta\delta/R)^2}\int_0^\eta \eta f'\,d\eta - \delta U_m\frac{\partial U_m}{\partial x}\frac{1}{R^2(1+\eta\delta/R)^2}\int_0^\eta f\,d\eta$$
$$- 2\frac{U_m^2}{\delta}\frac{\partial \delta}{\partial x}\frac{\eta f f'}{R(1+\eta\delta/R)} + 2U_m\frac{\partial U_m}{\partial x}\frac{f^2}{R(1+\eta\delta/R)} - U_m^2\frac{\partial R}{\partial x}\frac{f^2}{R^2(1+\eta\delta/R)^2}$$
$$= -\frac{U_m^2}{\delta^2}\left(1+\eta\delta/R\right)g_{12}''(\eta) - \frac{3}{R}\frac{U_m^2}{\delta}g_{12}'(\eta)$$

If the flow is self preserving the functions $f(\eta)$, $g_1(\eta)$, $g_2(\eta)$ and $g_{12}(\eta)$ are independent of x and thus the solution of Eq. (12)

requires that the coefficients of the universal functions be either non-zero constants or zero. The nonrepetitive coefficients of Eq. (12) are

$$\frac{U_m^3}{\delta^2}\frac{\partial\delta}{\partial x}\ ,\ \frac{U_m^2}{\delta}\frac{\partial U_m}{\partial x}\ ,\ \frac{U_m^2}{R\delta}\frac{\partial\delta}{\partial x}\ ,\ \frac{U_m}{R}\frac{\partial U_m}{\partial x}\ ,\ \frac{U_m^2}{R^2}\frac{\partial\delta}{\partial x}$$

$$\frac{\delta U_m}{R}\frac{\partial U_m}{\partial x}\ ,\ \frac{U_m^2}{R^2}\frac{\partial R}{\partial x}\ ,\ \frac{U_m^2}{\delta^2}\ ,\ \frac{U_m^2}{\delta R} \qquad (13)$$

Let

$$U_m(x) = Ax^m$$

$$\delta(x) = Bx^n \qquad (14)$$

$$R(x) = Cx^p$$

Substituting from Eq. (14) in each of the terms in (13), for each of these coefficients to be a non-zero constant (for a non-trivial solution) it is required that the exponents of x for each term are zero. This leads to the requirement that

$$\begin{aligned} 3m - n - 1 &= 0 \quad (a)\\ 2m - p - 1 &= 0 \quad (b)\\ 2m - 2p + n - 1 &= 0 \quad (c)\\ 2m - 2n &= 0 \quad (d)\\ 2m - p - n &= 0 \quad (e) \end{aligned} \qquad (15)$$

This is, five equations for the three unknowns m, n, p.

For the present, considering the slope of the gradient of the shear negligible, that is $g'_{12} \simeq 0$, allows Eq. (15d) to be eliminated. Then forcing Eq. (15e) to the form of Eq. (15b) gives rise to the condition that

$$g'_{12} \propto \frac{\partial\delta}{\partial x}$$

and

$$m = 0$$

$$n = 1$$

$$p = -1$$

The condition that $m = 0$ is that $U_m(x) =$ constant. Experimental evidence, to be discussed later, does not substantiate this condition at all. It is apparent that the term in Eq. (12) containing the slope of the gradient of the shear cannot be neglected, that is, $g'_{12} \neq 0$ and this fact is borne out by the experimental results obtained.

Sawyer [7] considering the viscous stress terms as negligible in comparison with turbulent shear stresses, obtained a similarity condition for Eq. (1). It is to be noted that the flow in the outer part of a two dimensional, curved, turbulent wall jet is approximately self preserving if the ratio of jet thickness to wall radius of curvature is constant along the jet. For a jet blowing over a surface this condition is satisfied for a logarithmic spiral profile only.

III. EXPERIMENTAL EQUIPMENT AND PROCEDURE

A. EXPERIMENTAL APPARATUS

Figure 1 shows the arrangement of the experimental apparatus. The general operation of the apparatus is given below.

Air passing through a 10 micron filter, at approximately 120 psig, was supplied to the apparatus through a one inch stop valve and pressure regulator. From the regulator the air was directed into the power jet of the test section through an appropriately sized Fisher-Porter Rotameter and a length of 3/4" I.D. plastic tubing.

A two-channel Constant-Temperature Hot Wire Anemometer (DISA-55D01) was used in making both mean velocity and turbulence measurements. A single wire and two cross wire (UV and UW) directional probes attached to a micrometer traverse were used to measure the velocity and turbulence profiles.

B. TEST SECTION

The test section was fabricated from a 2-1/2" sheet of plexiglass placed between two half-inch sheets of plexiglass (see Figures 2 and 3). The lower section of the power jet and the test section were machined in one piece. The quadrant was of radius three inches. The upper section of the power jet was machined from a 2-1/2" sheet of plexiglass to suit. The faces in contact with the fluid were given a final hand polishing.

The two side plates were made of 1/2" plexiglass sheets. A circular slot for the hot-wire mounting was machined in both side plates. These slots have a common center of curvature with the quadrant to ensure consistent radial settings of the wire.

The two sections of the power jet were then dowelled to one of the side plates to form the power jet of width 2-1/4" and length 9", converging to a 1/4" width over the length of half inch from the entrance

to the quadrant. The test section was completed by placing the other side plate on top of the power jet and quadrant sections and bolting the resulting assembly together.

C. PROCEDURE

Each run consisted of first selecting a flow rate. Then the appropriate D.C. and A.C. voltages were recorded at intervals from the surface cf quadrant up to 1.5 inches. The interval between readings was .010 inch nearer the surface and at positions where sudden changes in voltages were noted; elsewhere it was 0.050 inch. Runs were carried out every 15 degrees, from 5 to 65 degrees, along the quadrant for every flow rate.

The flow rate was established with Fisher-Porter rotameters of capacity 19.8 SCFM and 76.8 SCFM at 100%.

Flow rates corresponding to 95% of the full capabity on the 19.8 SCFM and 55% of full capacity on the 76.8 SCFM rotameters were used. These flow rates resulted in Reynolds numbers, based on the power jet width of 1/4", of 9340 and 21040 respectively. (The latter is the more common Reynolds number used in association with fluidic amplifiers.)

Calibration of each wire utilized was performed using a Model 1125 Calibrator manufactured by Thermo-Systems, Inc. Calibration curves were drawn for each wire used. The intercept (V_o^2) and slope (B) from the linear calibration curve drawn were used in subsequent calculations.

D. DATA REDUCTION

The following procedure was used in the reduction of the test data:

The flow rate in standard cubic feet per minute was first calculated by using Q(SCFM) = Rotameter reading x 100% full flow capacity

$$\times\ CF(T) \times CF(P)$$

where

CF(T) = atmospheric temperature correction factor

and

CF(P) - atmospheric pressure correction factor.

The correction factors were obtained from the Fisher-Porter instruction manual.

Next the average velocity in the nozzle was calculated from

$$U_o \text{ (ft/sec)} = \frac{Q}{A_c}$$

where

A_c = cross sectional area of the nozzle.

The Reynolds number was calculated as $Re_w = \frac{U_o W}{\nu}$. All fluid properties were evaluated at 14.7 psia and 70°F.

The normalized velocity profiles were obtained by plotting $\frac{u}{U_m}$ against $\frac{y}{R}$ where U_m was the maximum fluid velocity in a given profile. y was the radial distance from the surface of the quadrant and R was the radius of the quadrant. The turbulence intensities $\frac{u'}{u}$, $\frac{v'}{u}$, $\frac{w'}{u}$ and the distribution of the $\overline{u'v'}$ and $\overline{u'w'}$ correlation were also plotted against $\frac{y}{R}$.

Normalized velocity profiles, turbulent intensities and $\overline{u'v'}$ and $\overline{u'w'}$ correlations were also plotted against $y/y_{m/2}$ where $y_{m/2}$ is the radial distance from surface to point where $u = 0.5\ U_m$.

IV. DISCUSSION OF EXPERIMENTAL RESULTS AND CONCLUSIONS

Measurements of mean velocities, turbulence intensities u', v', w' and turbulent shear stress distributions $\overline{u'v'}$, $\overline{u'w'}$ were performed. A single wire probe and two cross wire probes (uv and uw configurations) were utilized. It was possible to measure to within 0.010 inch from the surface of the quadrant with the single wire and the uw cross wire probes. The closest point of measurement from the surface for the uv cross wire was 0.060 inch.

The mean velocity profiles obtained using the three sets of wires independently were in close agreement ($\pm$5 per cent) with each other at corresponding angular positions. This indicates that a very high degree of reliability can be placed upon the experimental data obtained.

Figures 4 and 5 show the mean velocity profiles, for the two Reynolds numbers tested, plotted non-dimensionally with respect to the maximum profile velocity U_m and the radius of the quadrant R. These plots show that for any angular position the velocity profiles for the two flow rates coincide convincingly for any value of y/R, thus indicating that for the flow rates considered the flow spread parameters y_m and $y_{m/2}$ are independent of the Reynolds number. The kinks occurring in the θ = 5 degs. curves are attributed to the effect of the upper wall of the nozzle upon the flow issuing from it.

Figure 6 shows the mean velocity distribution for Re_w = 9340 at 15 degree intervals along the midplane for θ = 5 to 65 degrees. It is to be noted from the similarity in all jet profiles that the jet remains attached even at 65 degrees. Figure 7 is the velocity profiles of the flow at θ = 5 degree position at 5 stations across the length of the nozzle. The close approach to a two dimensional flow pattern is seen

from the relatively small changes noted throughout the traverses. This is particularly so for the middle of the section.

In an attempt to determine the mean velocity similarity parameters the non-dimensional mean velocity profiles for the 35 and 65 degree angular positions for the two Reynolds numbers were plotted as shown in Fig. 8. Also shown on this figure is the theoretical curve predicted for the outer region of a free jet by Glauert [8] as given by

$$\frac{u}{U_m} = \operatorname{Sech}^2\left[0.88\left(\frac{y}{y_{m_{\frac{1}{2}}}}\right)\right], \qquad \left(y \geq y_m\right)$$

There is good agreement with the theory for the outer region with some divergence for $y/y_{m/2} > 1.2$. This divergence may be attributed to the unstable nature of the outer region and to the centripetal effects due to the curvature in a wall jet flowing over a convex surface. It is well to note Glauert's caution, in such comparisons, that agreement between experimental data and his calculated profiles does not necessarily mean that the assumptions made by him about the constancy of shear stress distribution in this region were correct. In fact, Richardson [3] showed that agreement with Glauert's theory in the case of a plane wall jet flow in the outer region was mainly due to the loss of momentum in this region being very small. Furthermore, Sawyer [14], on the basis of a first order mixing length theory, indicates that entrainment can also contribute to a deviation in the velocity profile for a curved jet as compared to that of the plane jet case.

Figures 9a and 9b show the growth of the jet around the surface of the quadrant. In Fig. 9a two markedly distinctive growth patterns are portrayed--the first, 5 to 35 degrees, being governed by entrainment effects while the second, 35 to 65 degrees, being governed more by curvature and wall effects. This case is in stark contrast to those

of Fekete and Sawyer which show a constant growth pattern throughout. Figure 9b shows the difference existent between the growth of a free and a curved wall jet. Again, two distinct growth patterns are portrayed for the curved wall jet compared to the constant growth of the free jet.

The turbulent intensities are shown grouped for discussion purposes in Figs. 10 - 12, 13 - 15, 16 - 18, 20 - 22, and 23 - 25. The first graph in each group displays the local turbulence intensity figures; the following two graphs show the analogous turbulence intensity for each of the two Reynolds numbers tested non-dimensionalized with respect to the maximum profile velocity, U_m and the jet growth parameter, $y_{m/2}$. The amazing orderliness wrought by this particular non-dimensionalizing is striking.

The kinks apparent in all the local turbulence intensity curves at the 5 degree position again arise from the effect of the upper nozzle lip upon the issuing jet.

The turbulent intensities at the lower Reynolds numbers are larger than those at the higher ones, as would be expected, due to the more complete mixing effected at the lower velocity which enables turbulent energy to be cross transferred more freely.

The relative order of magnitude of the local turbulence intensities is $u' > v' \simeq w'$. The intensities are largest where the turbulent shear is maximum and reach their minimum values where the mean velocity is maximum; these intensities begin with a non-zero value close to the wall.

These figures also show that the maximum turbulent intensities occur closer to the surface of the quadrant for increasing Θ indicating a stabilizing effect due to the growth of the inner layer. This trend is the reverse of that observed by Margolis and Lumley [12] in an enclosed curved channel. It must be noted, however, that the Margolis data is non-dimensionalized with a constant characteristic

length whereas herein $y_{m/2}$, which increases monotonically with θ, is used to non-dimensionalize the data.

The turbulent intensities are high up to a value of $y/y_{m/2} \simeq 1.6$ for the 35 and 65 degree angular positions due to the turbulent energy produced near the surface, where shear rates are high, being transported by centripetal effects to regions where the local production is small.

Guitton [7] found that the longitudinal turbulent intensity increased from concave to plane flow and from plane to convex flow. Figure 19 shows the local longitudinal component for the wall jet on a concave surface as obtained from Guitton and that for the convex surface under investigation. It is evident that the local longitudinal turbulence intensity does indeed increase, although the angular position and Reynolds number tested for the concave surface are much higher than those for the convex surface. Guitton hesitated to link this increase of intensity to the growth of the turbulent region as he did not have turbulent shear stress data available. The $\overline{u'v'}$ distributions shown in Figs. 21-22 and the turbulent intensities in Figs. 10-18 indicate the growth in the shear stress and in the anisotropy of the flow. Thus the increase in longitudinal turbulence intensity for the convex flow can be attributed to the growth of the turbulent region due to centripetal effects.

Of final noteworthiness in the turbulence intensity data is the radial turbulent velocity component distribution v'. At the higher Reynolds number, the magnitude of this component, non-dimensionalized with respect to U_m, is smaller than the other turbulent intensities due mainly to the overpowering effects of entrainment on the mean radial velocity.

Entrainment effects also appear in the lower Reynolds number data as affecting the dampening of the radial component, that is, the decay of this component is slowed due to entrainment mean velocity effects interacting with centripetal acceleration effects.

The measurements of turbulent correlations $\overline{u'v'}$ and $\overline{u'w'}$ are shown in Figs. 20 to 25. The $\overline{u'v'}$ correlation is positive throughout the flow. The curvature of the convex surface gives rise to the effects of centripetal acceleration which causes a negative v' to be associated with a negative u' resulting in a positive $\overline{u'v'}$ correlation. Further, the presence of a destabilizing effect, that is a negative gradient of angular momentum, as shown by Eskinazi and Yeh [16], which is associated with the outer part of the convex flow, combines to enhance the positive correlation.

In Figs. 21 and 22 the effect of the upper lip of the nozzle is again evidenced in the shear stress data for the 5 degree angular position, being more prominent in the high Reynolds number flow where the initial shear forces are higher.

Figures 23 - 25 show that the $\overline{u'w'}$ correlation varies from negative to positive values for the flow away from the surface of the quadrant. The overall average of $\overline{u'w'}$ tends toward zero as it should for a planar flow.

Of final note with respect to the $\overline{u'v'}$ shear stress data is the fact that this stress does not vanish where the mean velocity gradient is zero. This was also observed by Poreh, Tsuei and Cermak [15] in the case of a turbulent radial wall jet. Obviously the conventional eddy viscosity model $-\overline{u'v'} = \varepsilon \frac{\partial u}{\partial y}$ used in the plane surface cases cannot be applied here. Thus a model of eddy viscosity like that of Sawyer's is seen to be more appropriate to the case of curved turbulent flows.

In conclusion, the primary characteristics of a turbulent, two dimensional air jet flowing over a convex surface of constant radius are:

1. The entire mean velocity profile for $\theta \geq$ 35 degrees up to 65 degrees, as measured here, are similar, but the turbulent flow in this configuration is not self preserving. Thus the total flow is not self preserving. The mean velocity over

the field, however, is independent of the flow Reynolds number based on the nozzle width.

2. The overall level of turbulence is higher in a convex wall jet in comparison to that in a concave wall jet. This increase can be contributed to centripetal effects which enhance the transport of wall created turbulent energy to areas of low local energy production.

3. The local turbulent intensities are ordered such that $u' > v' \simeq w'$. However, maximum turbulence intensities occur closer to the surface for increasing distance along the surface, indicating the stabilizing effect of the convex wall.

4. Entrainment effects are most evidenced in the turbulent flow field by the dampening action of the entrained mean flow, in opposition to the centripetal effects of the geometry, upon the radial turbulence intensity distribution.

5. The inlet region, $\Theta < 35$ degrees, is a transition region wherein entrainment effects predominate, a fact strikingly evidenced by the difference between jet growth rates for the transition and the fully developed regions.

6. The turbulent shear stress term $\overline{u'v'}$ is positive throughout the flow and does not vanish where the mean velocity gradient is zero as shown in Figs. 21 and 22. Thus conventional eddy viscosity models cannot be applied to this flow field. The Reynolds stress term $\overline{u'w'}$ is small and has no overall effect upon the planar flow field.

V. RECOMMENDATIONS FOR FUTURE WORK

The foregoing investigation suggests that the following areas should be subject to further study:

1. Detailed examination of the transition region, $\theta \leq 35$ degrees, with respect to entrainment effects should be initiated.
2. Determination of an appropriate eddy viscosity model for curved wall jet flows should be made.
3. Analytical studies to determine a similarity condition for the equations of motion, with both laminar and turbulent shear stress terms included, should be continued.
4. The turbulent flow field in a plane inclined wall jet geometry should be investigated for comparison with the findings in this study.
5. The effects of setback and control opening upon turbulent flow field in this convex wall jet flow geometry should be studied with a view toward fluidic applications.

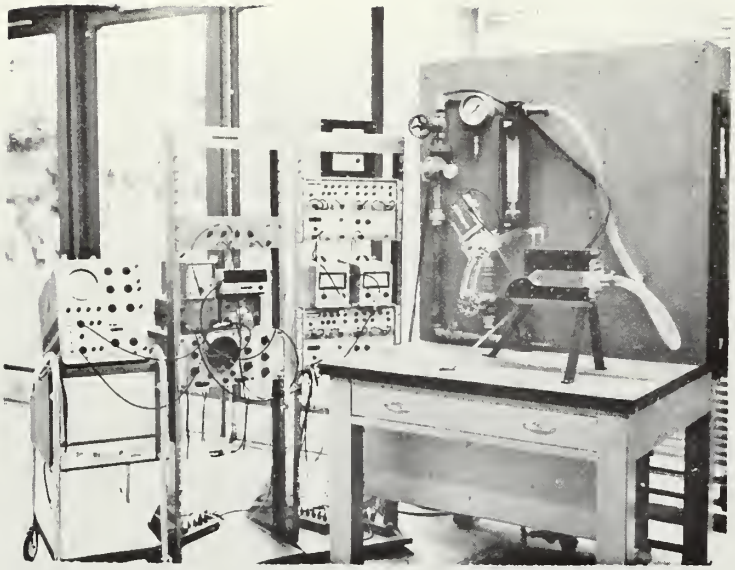

FIG. 1. Experimental Equipment

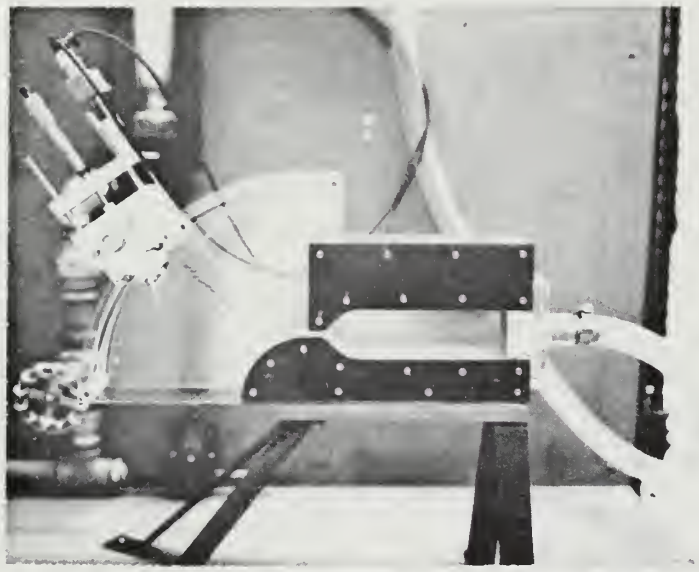

FIG. 2. Test Section

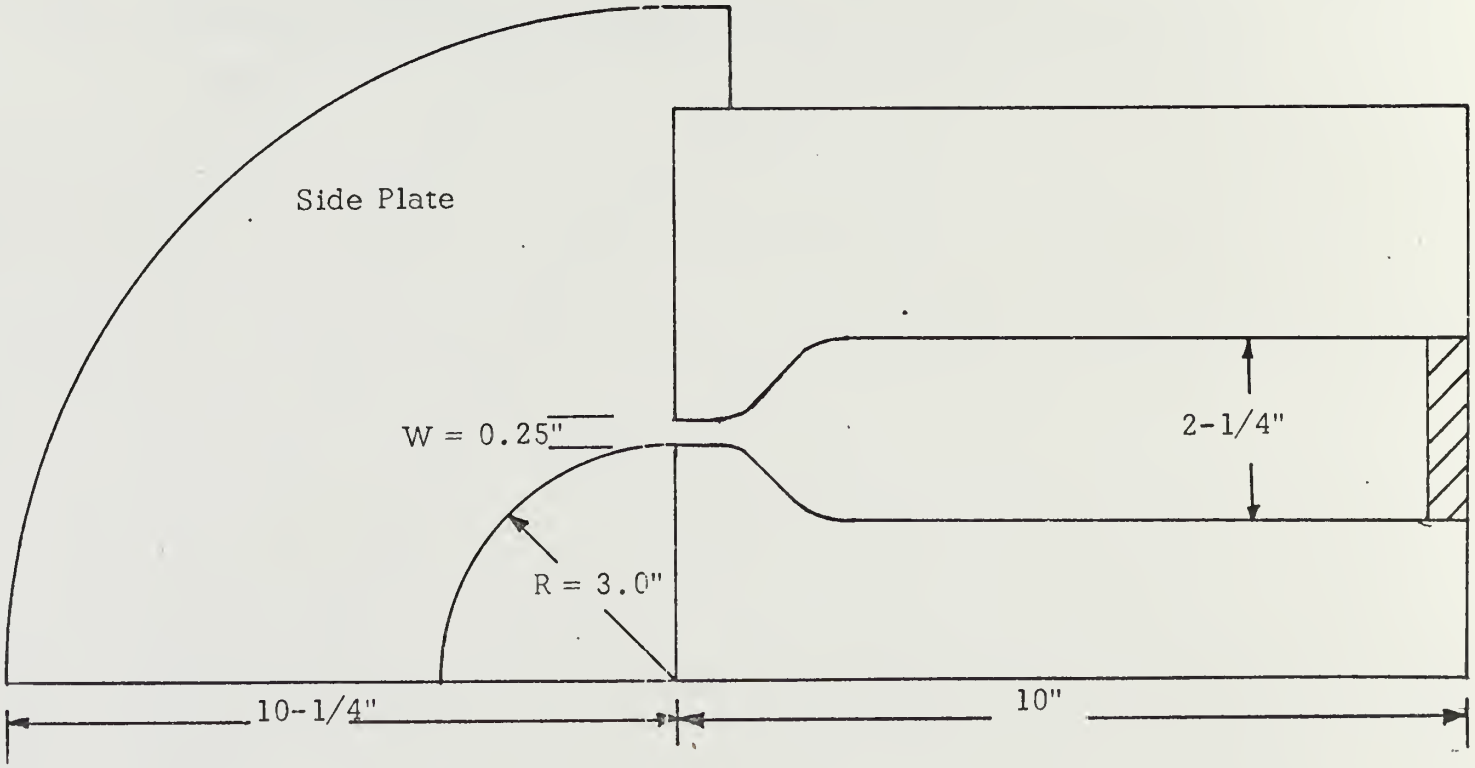

FIG. 3. Schematic of Test Section

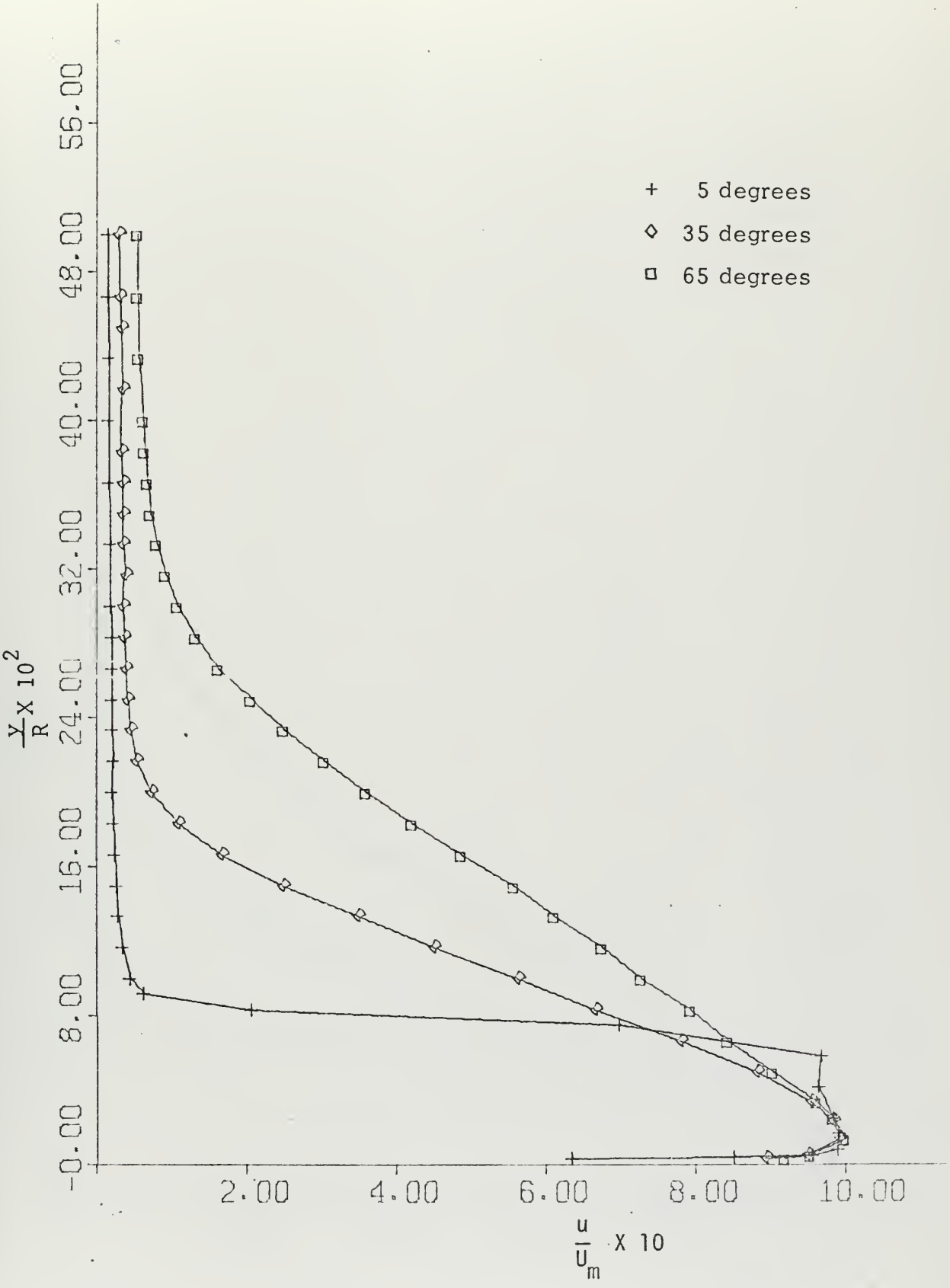

FIG. 4. Mean Velocity Distributions, $Re_w = 21040$

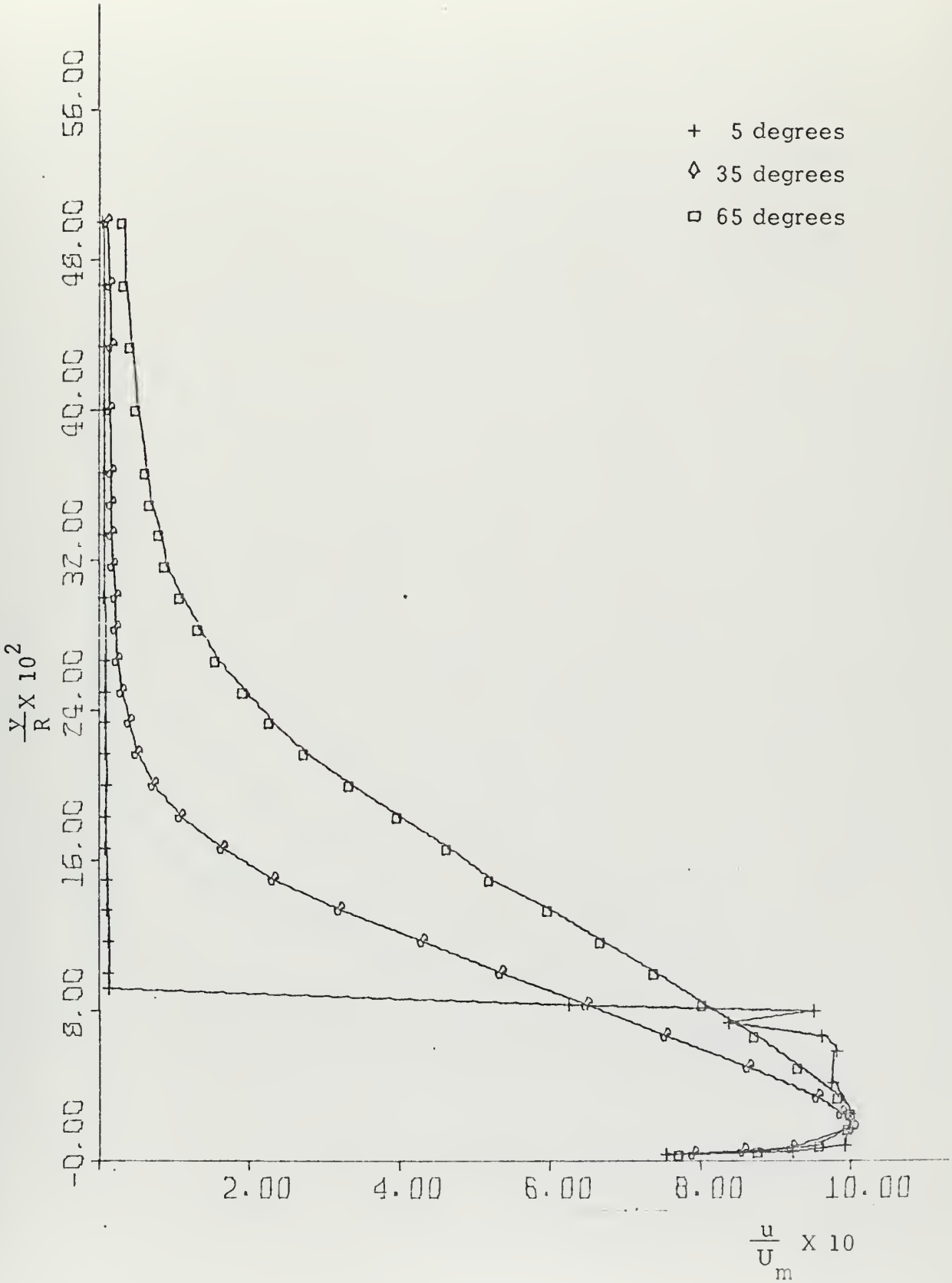

FIG. 5. Mean Velocity Distributions, $Re_w = 9340$

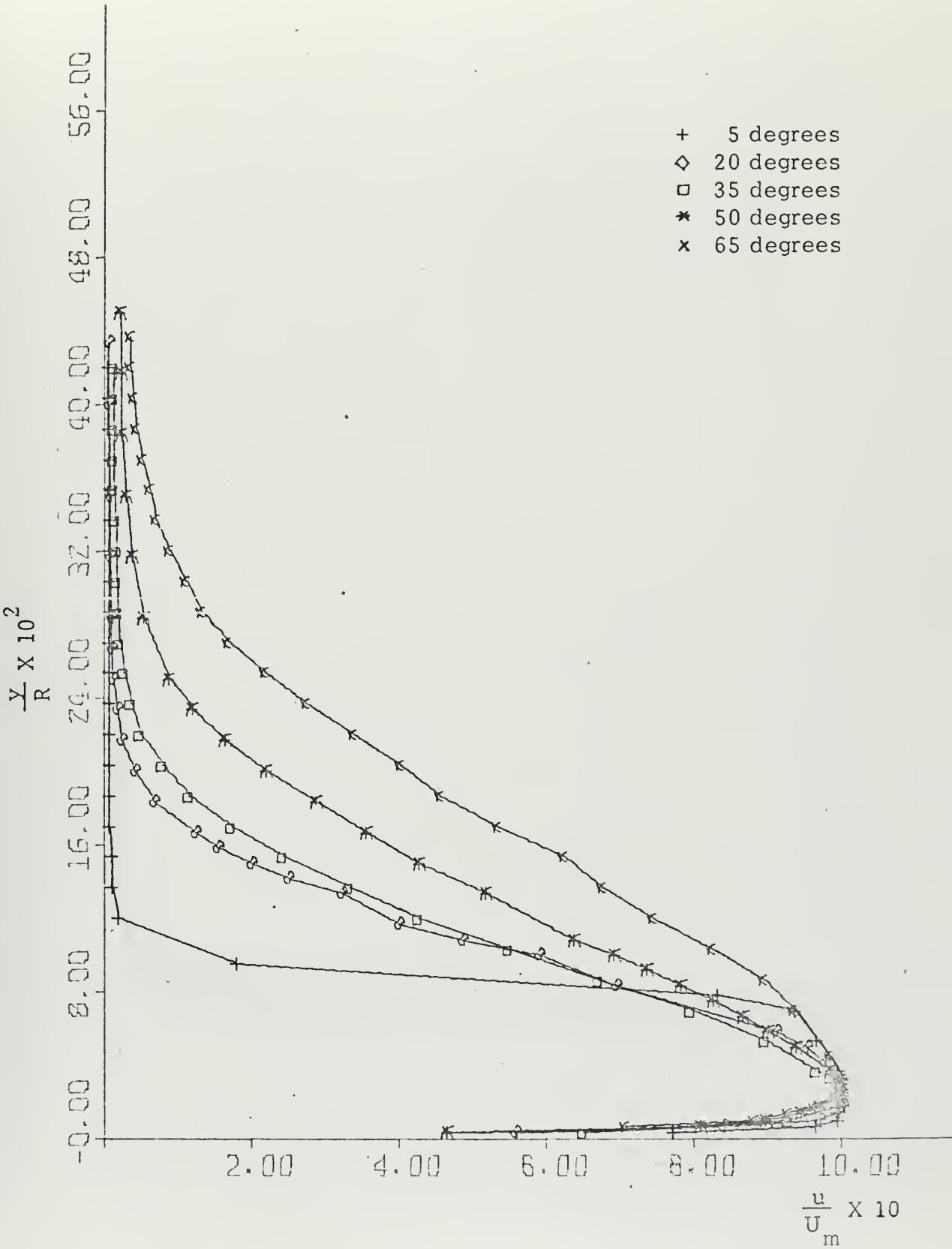

FIG. 6. Mean Velocity Distribubutions at 15 Degree Intervals, $Re_w = 9340$

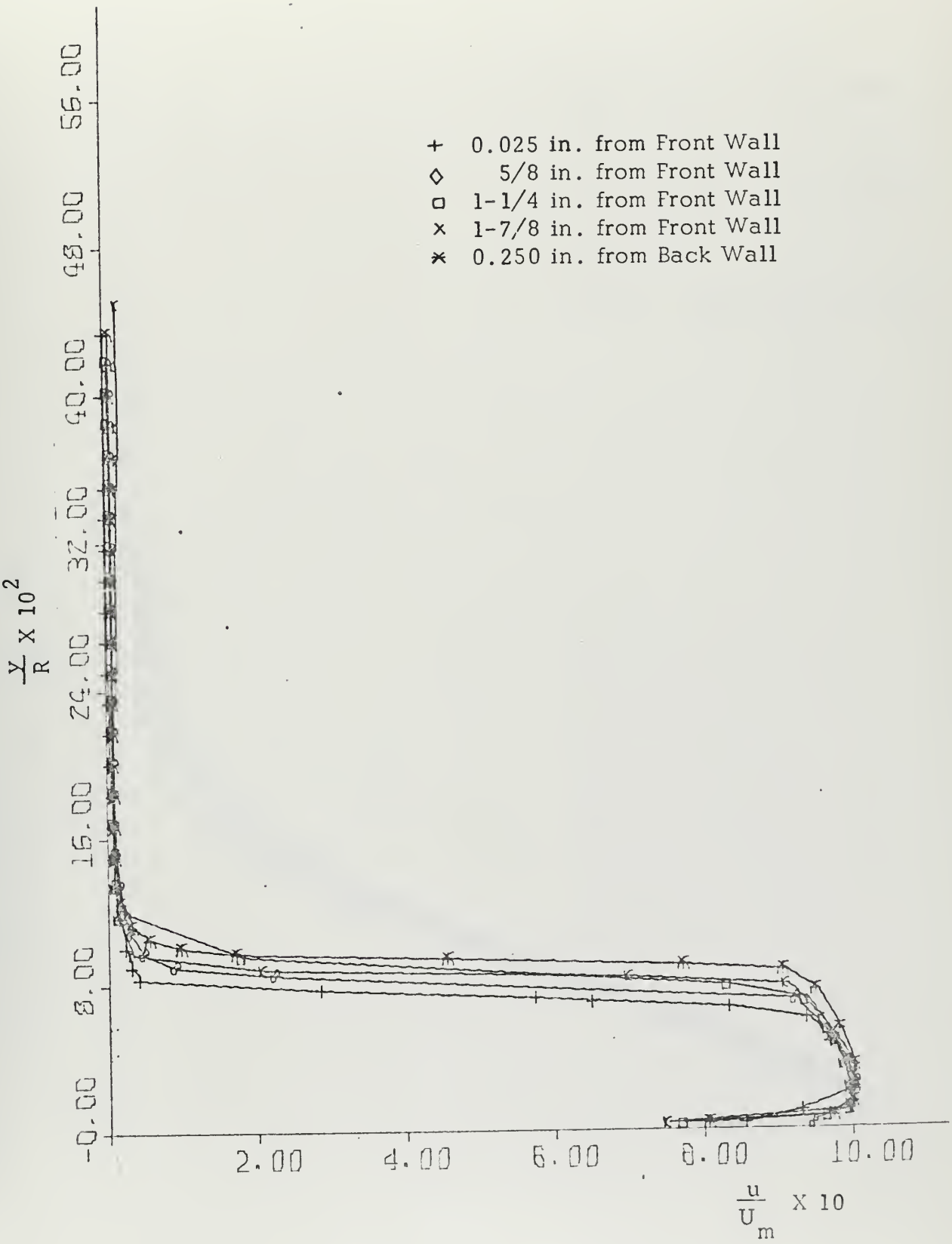

FIG. 7. Mean Velocity Distributions Across Nozzle at 0 = 5 Degrees
Re_w = 9340

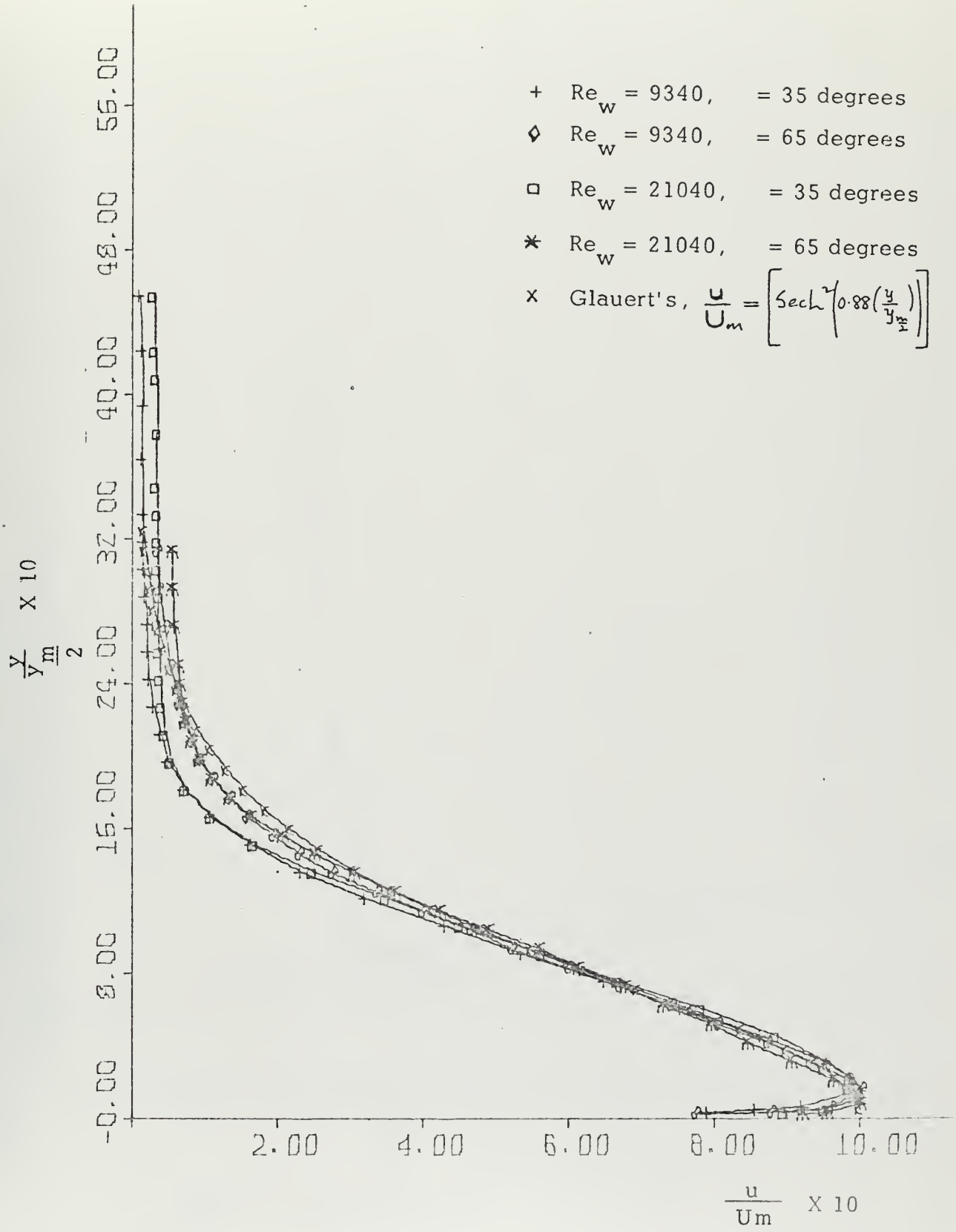

FIG. 8. Similarity in Mean Velocity Distribution

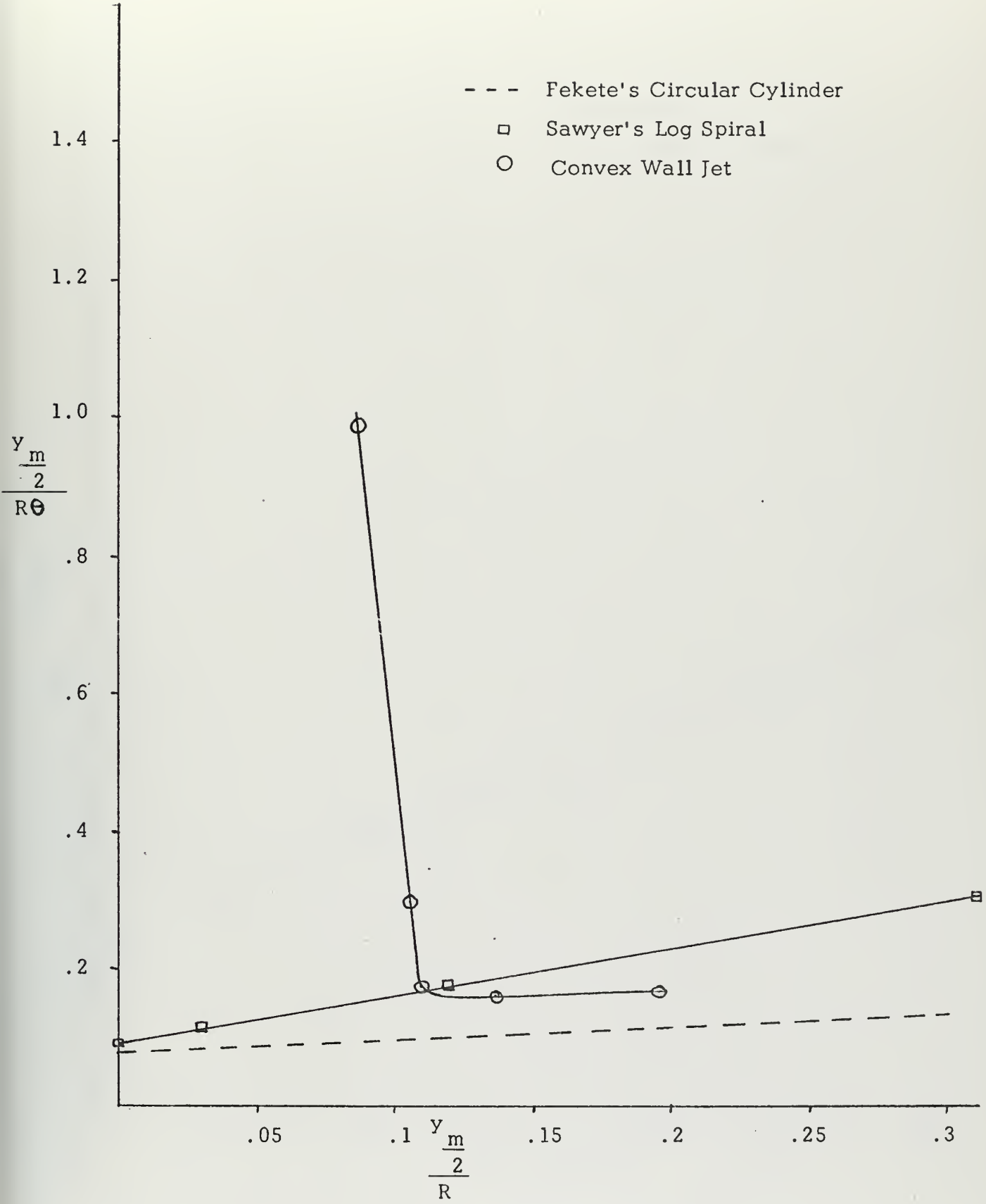

FIG. 9a. Jet Growth Rate

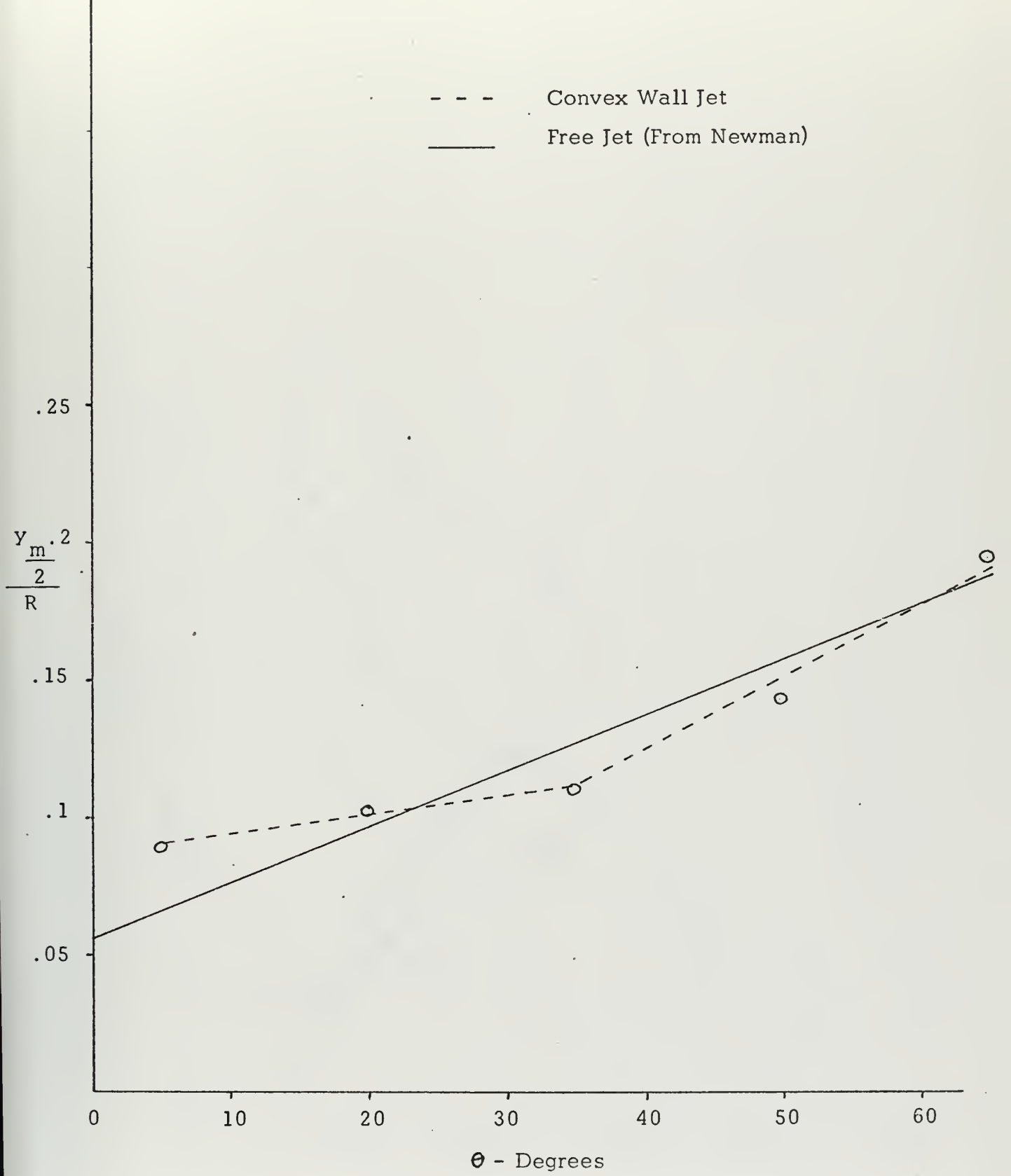

FIG. 9b. Growth of Jet Around Convex Wall, $Re_w = 9340$

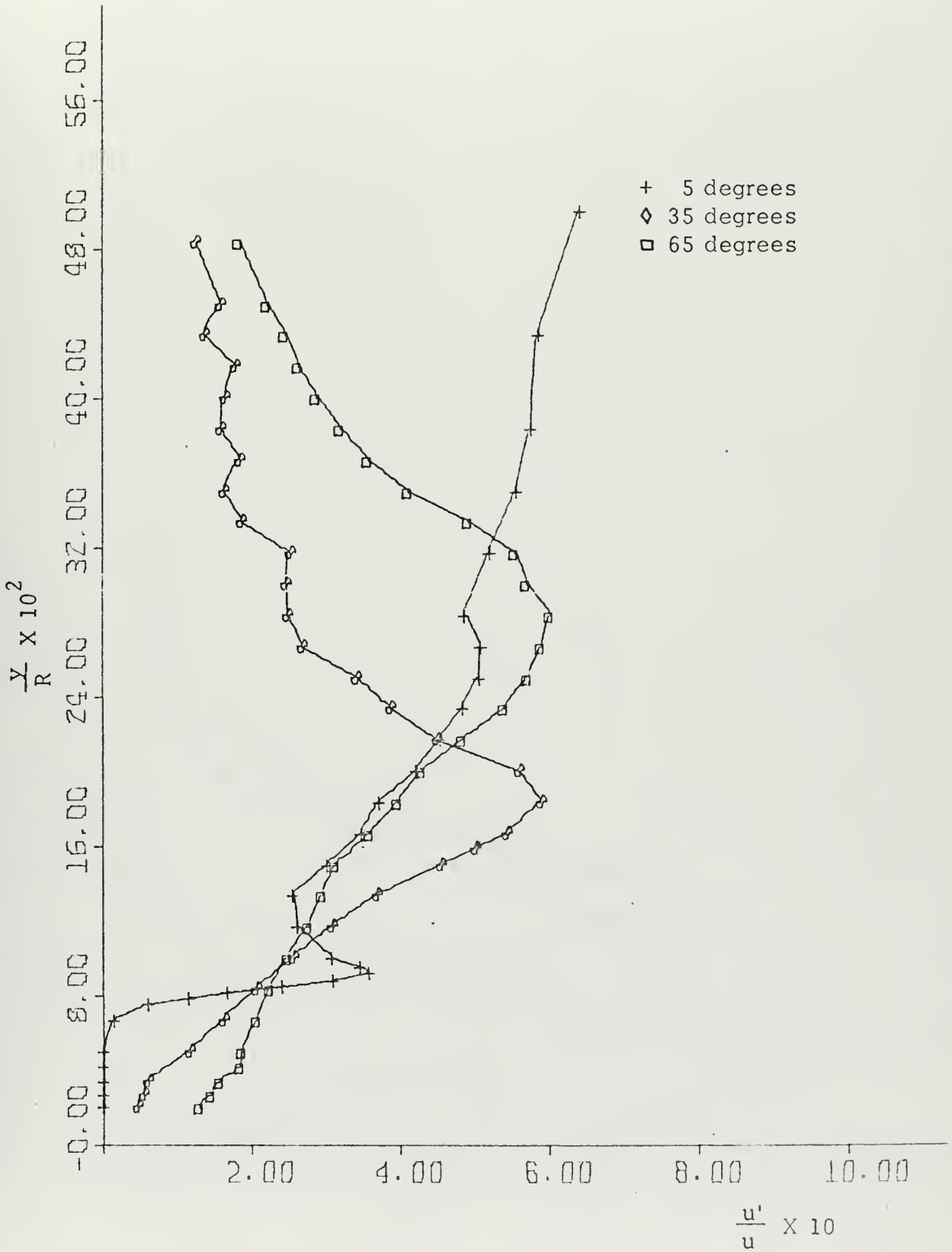

FIG. 10. Local Longitudinal Intensity of Turbulence, $Re_w = 21040$

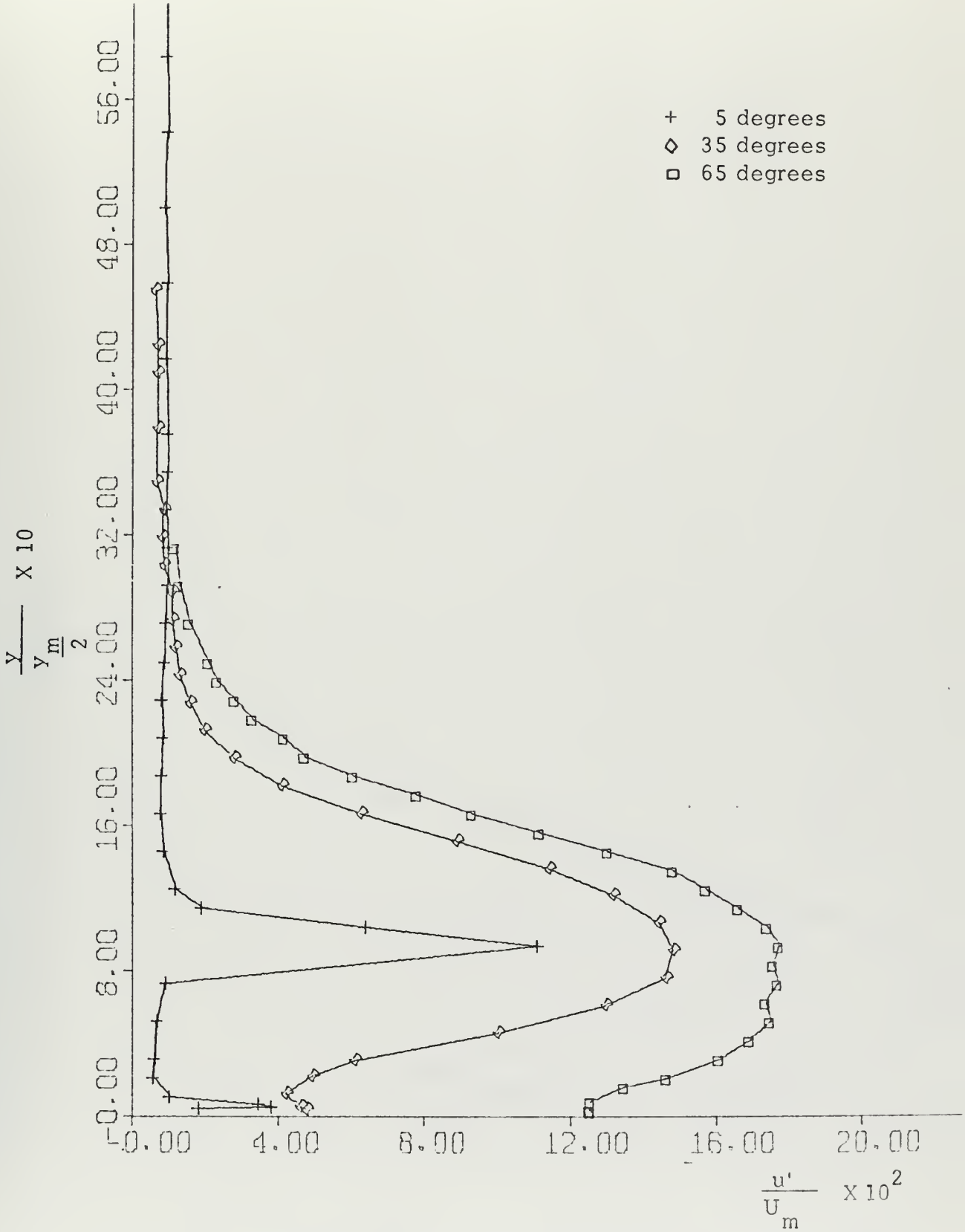

FIG. 11. Longitudinal Intensity of Turbulence, $Re_w = 21040$

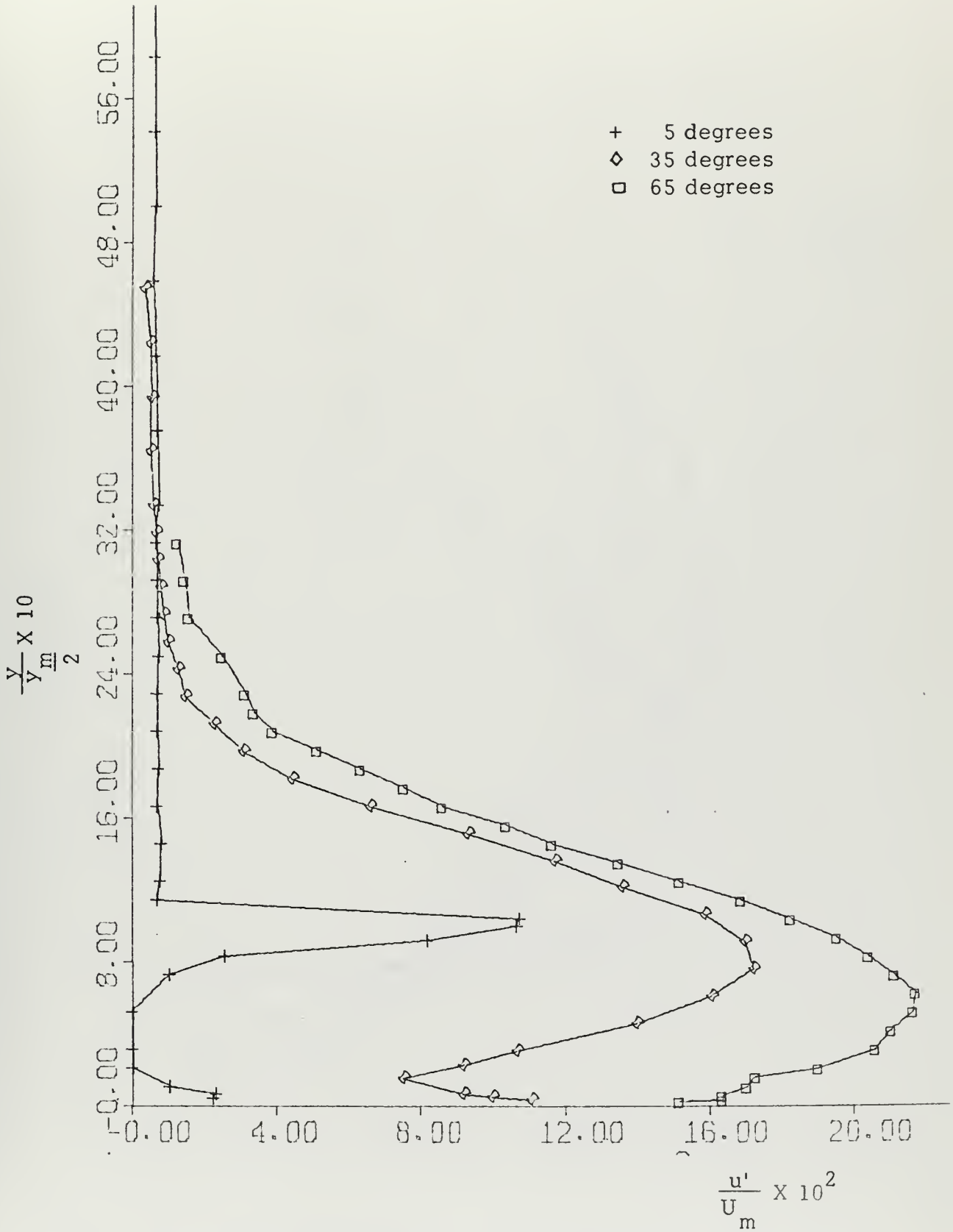

FIG. 12. Longitudinal Intensity of Turbulence, $Re_w = 9340$

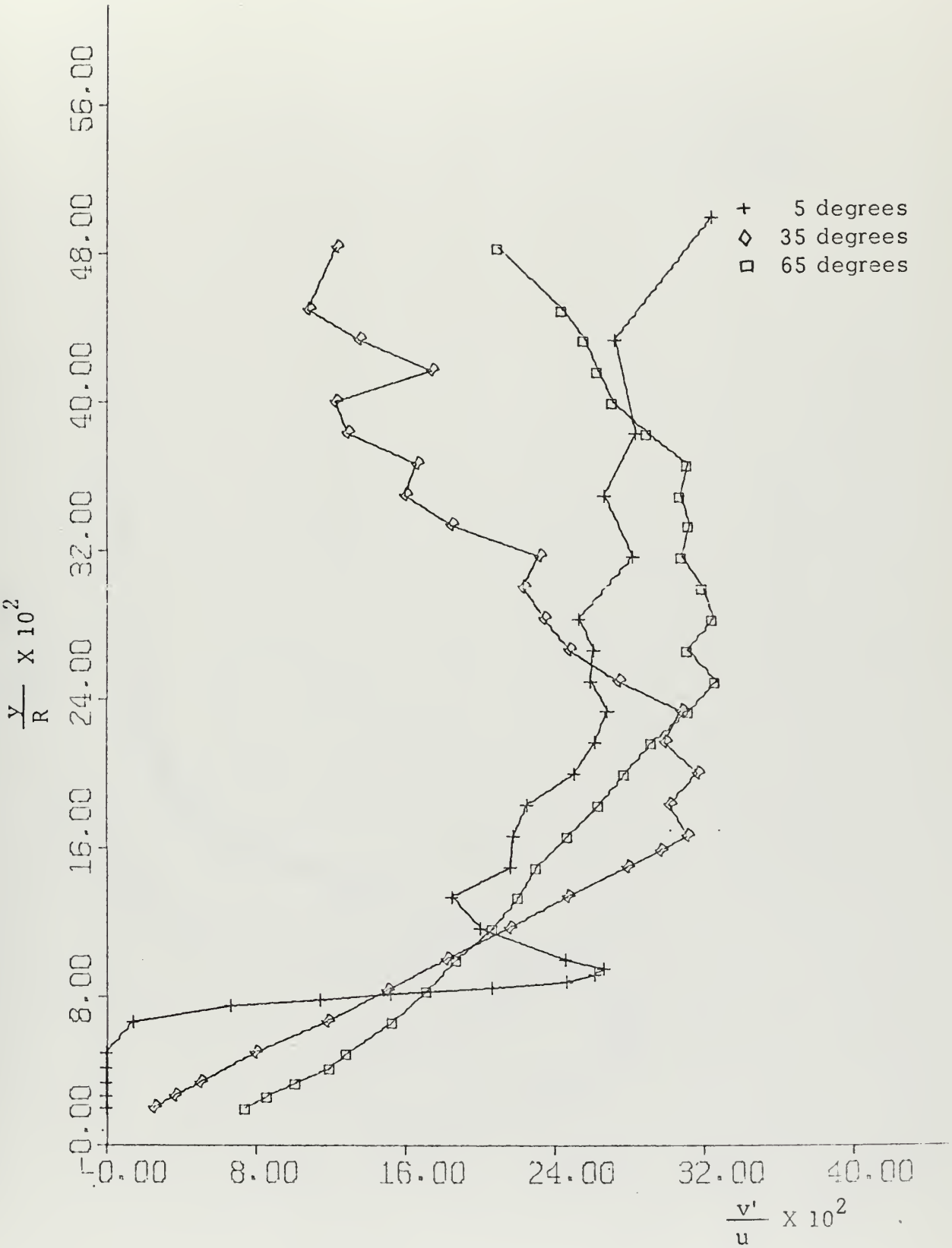

FIG. 13. Local Radial Intensity of Turbulence, Re_w = 21040

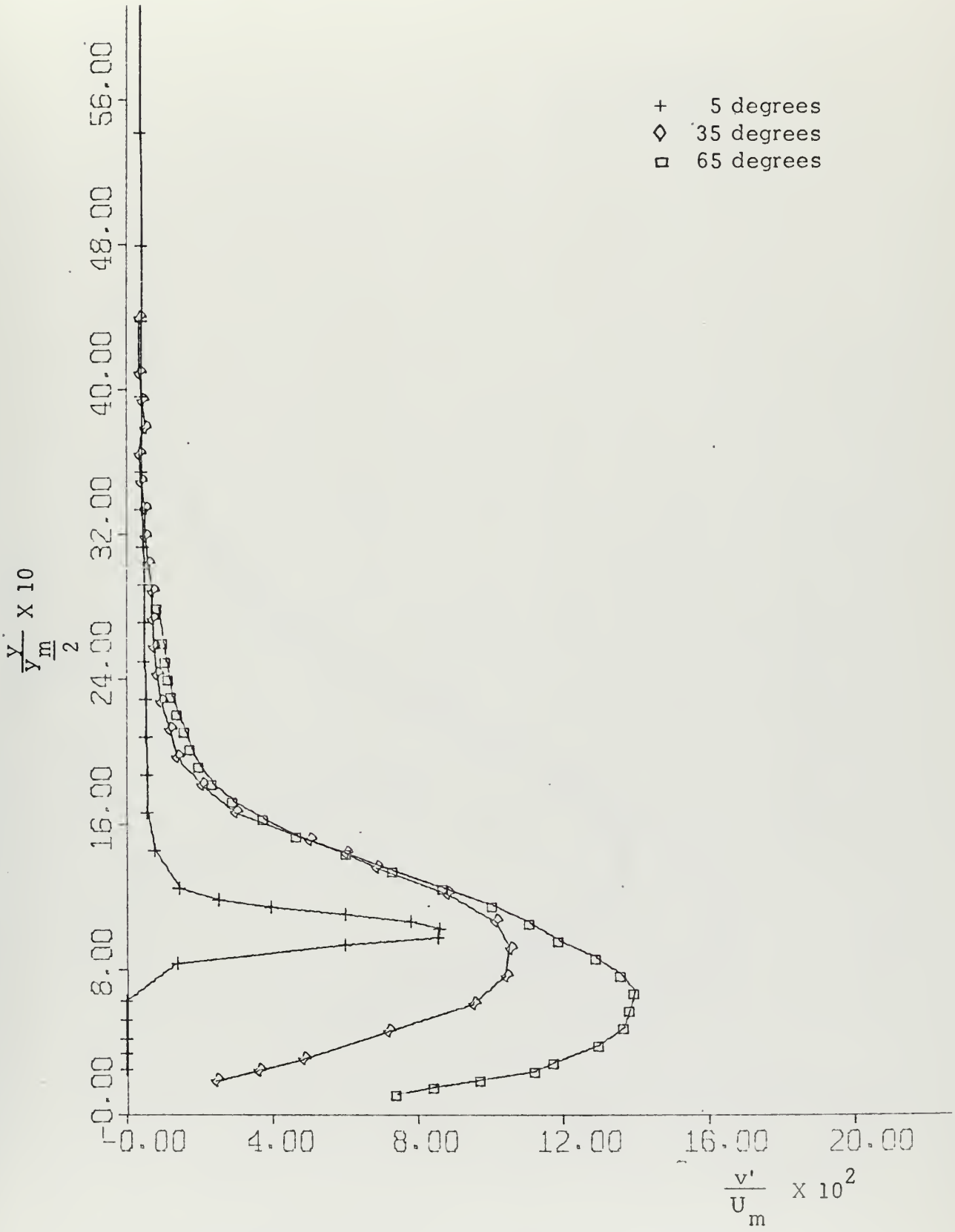

FIG. 14. Radial Intensity of Turbulence, Re_w = 21040

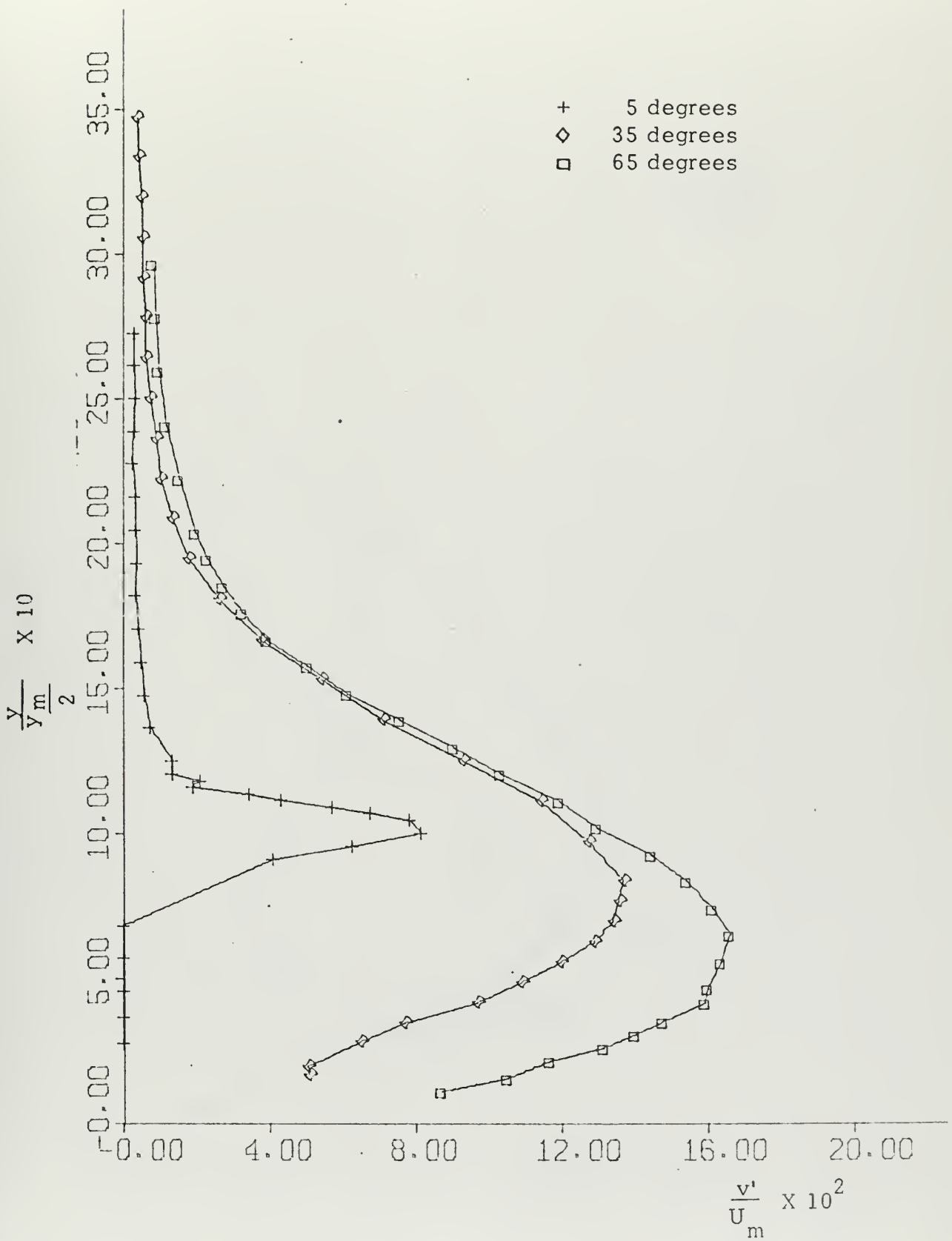

FIG. 15. Radial Intensity of Turbulence, Re_w = 9340

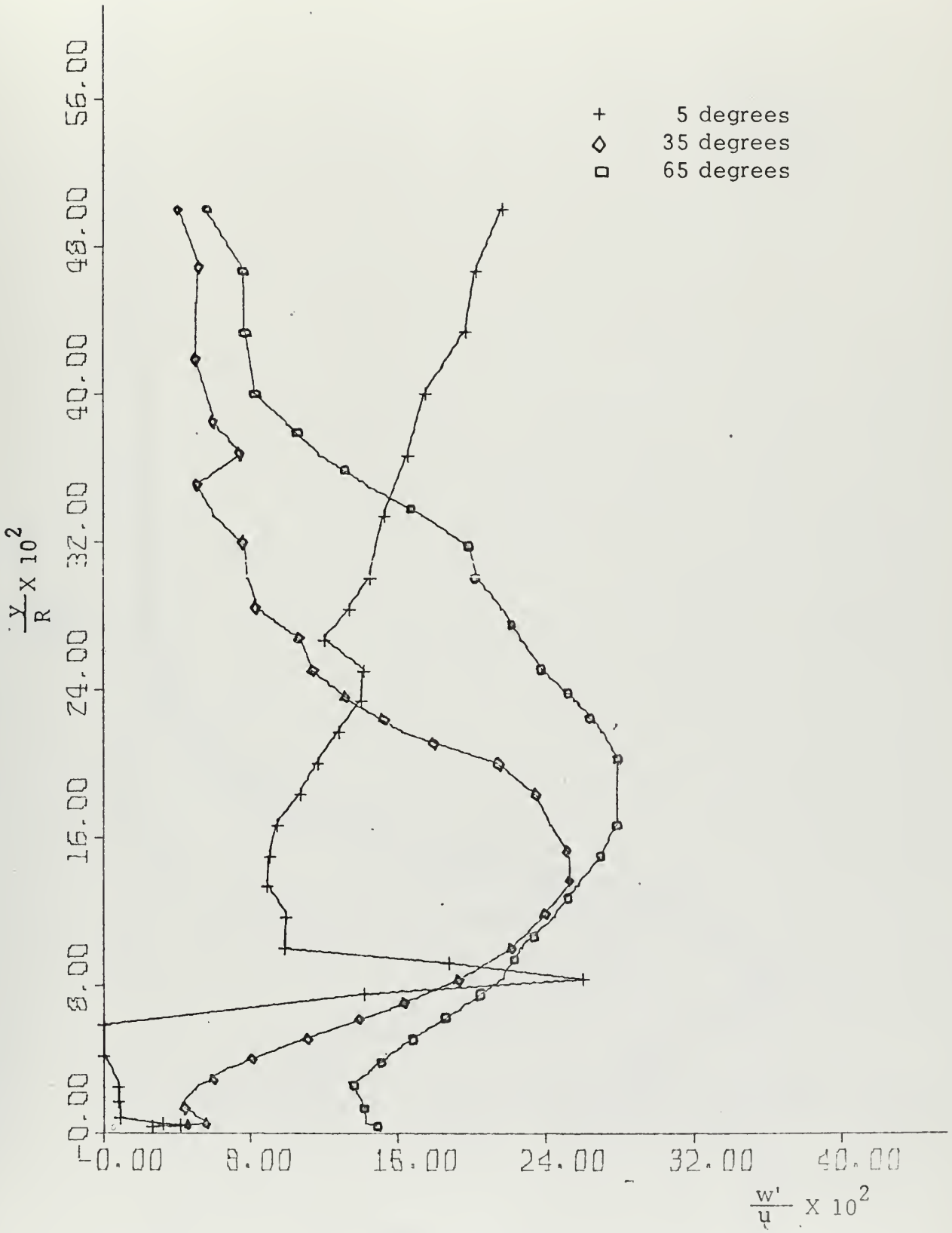

FIG. 16. Local Axial Intensity of Turbulence, $Re_w = 21040$

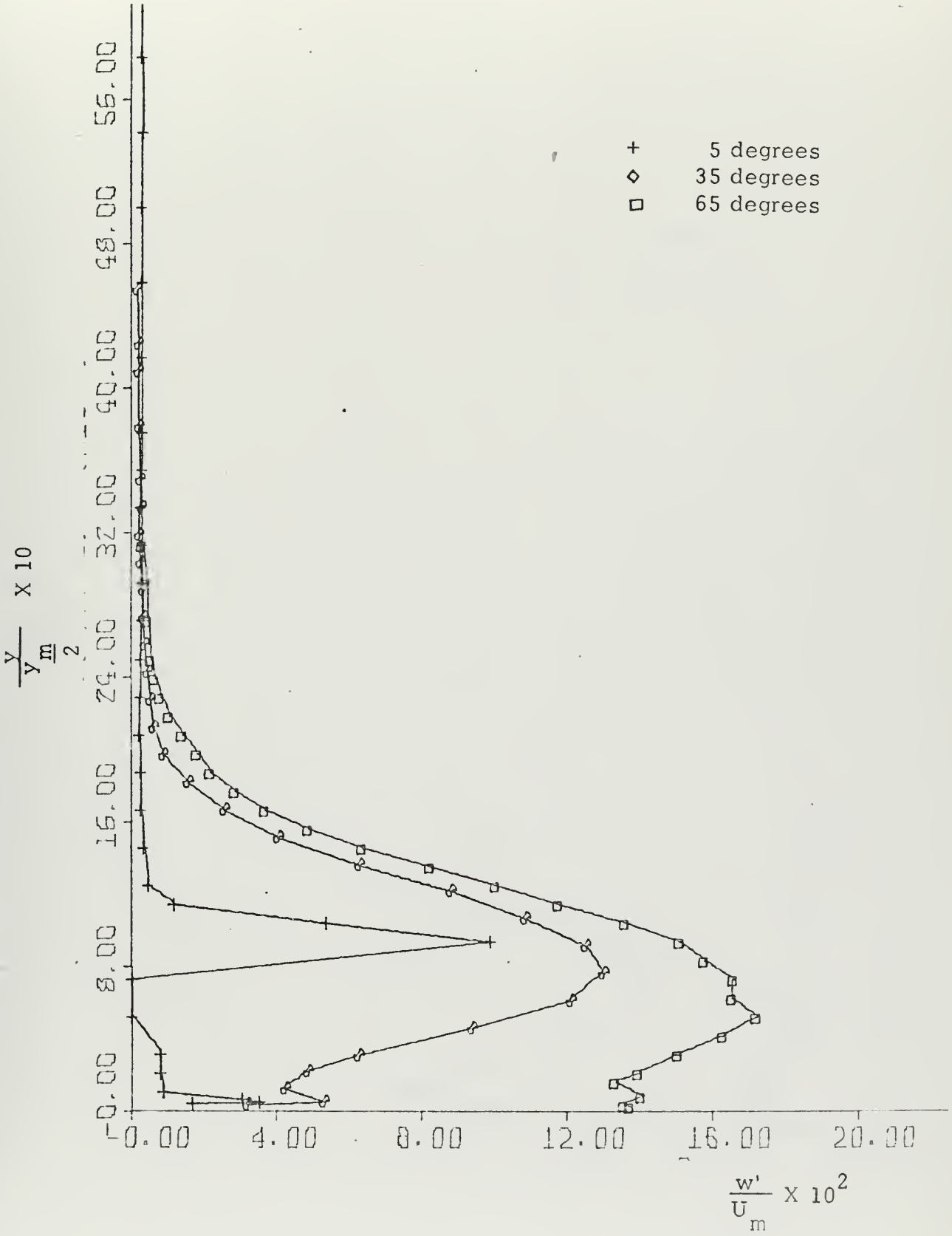

FIG. 17. Axial Intensity of Turbulence, $Re_w = 21040$

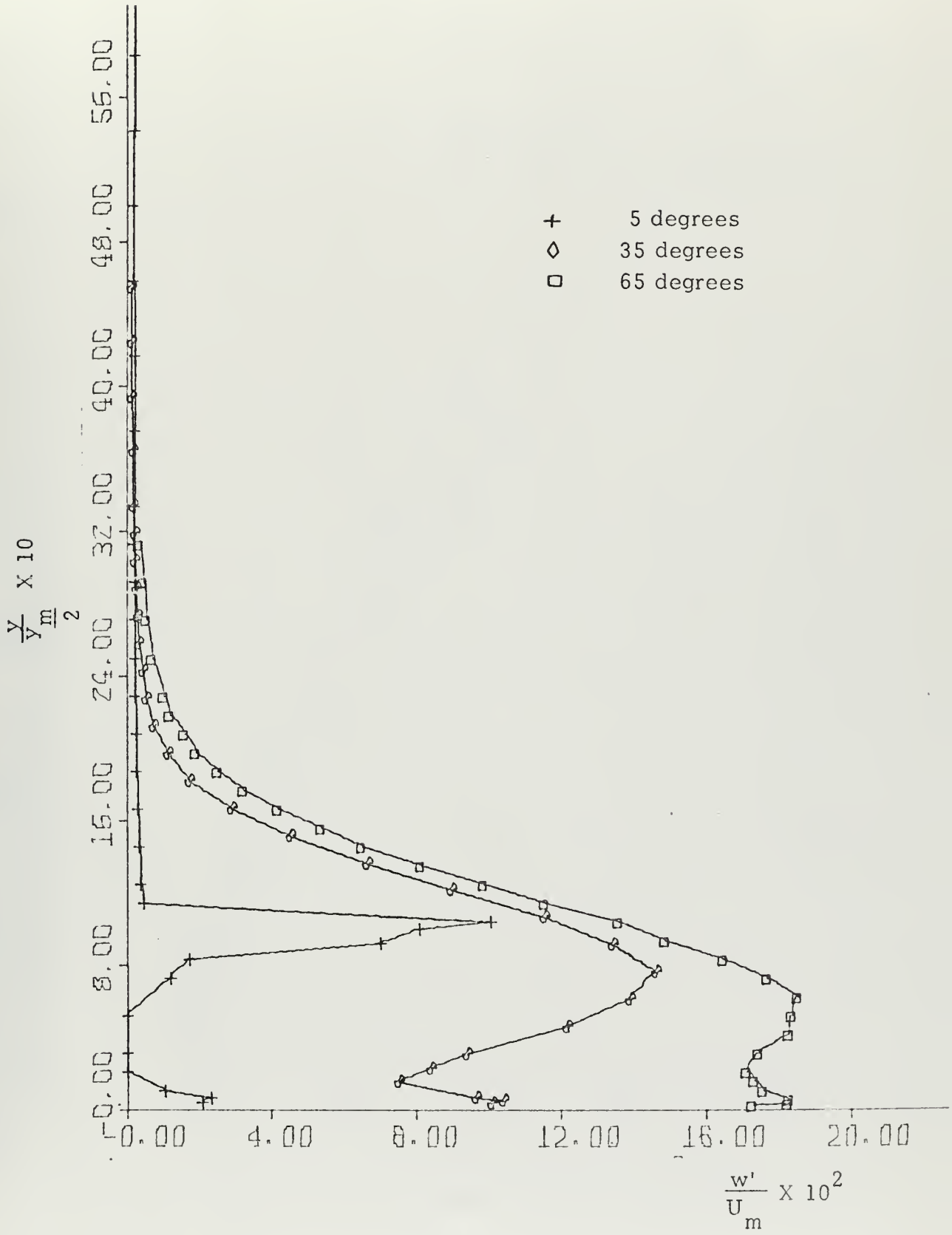

FIG. 18. Axial Intensity of Turbulence, Re_w = 9340

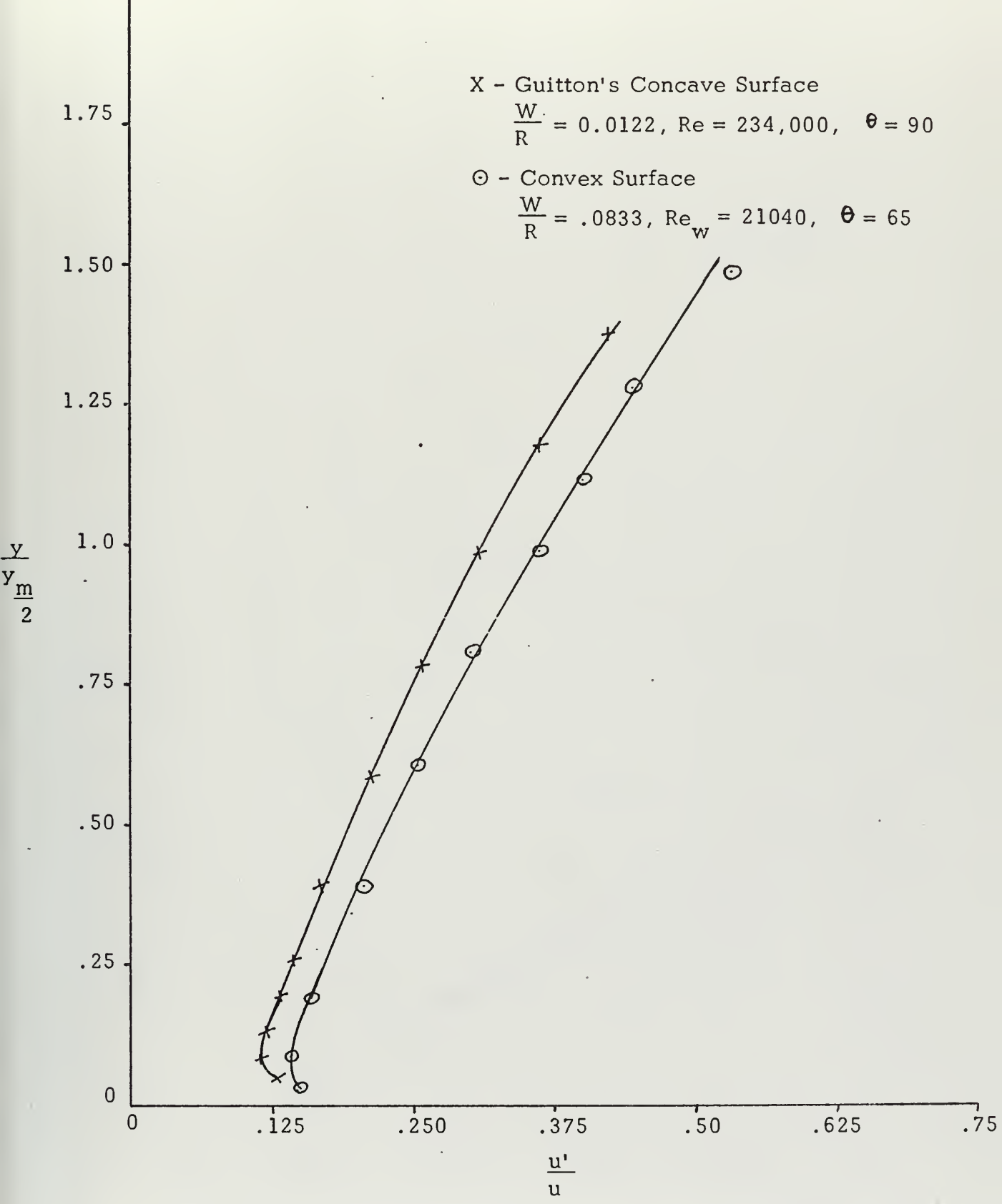

FIG. 19. Comparison of Longitudinal Intensity of Turbulence

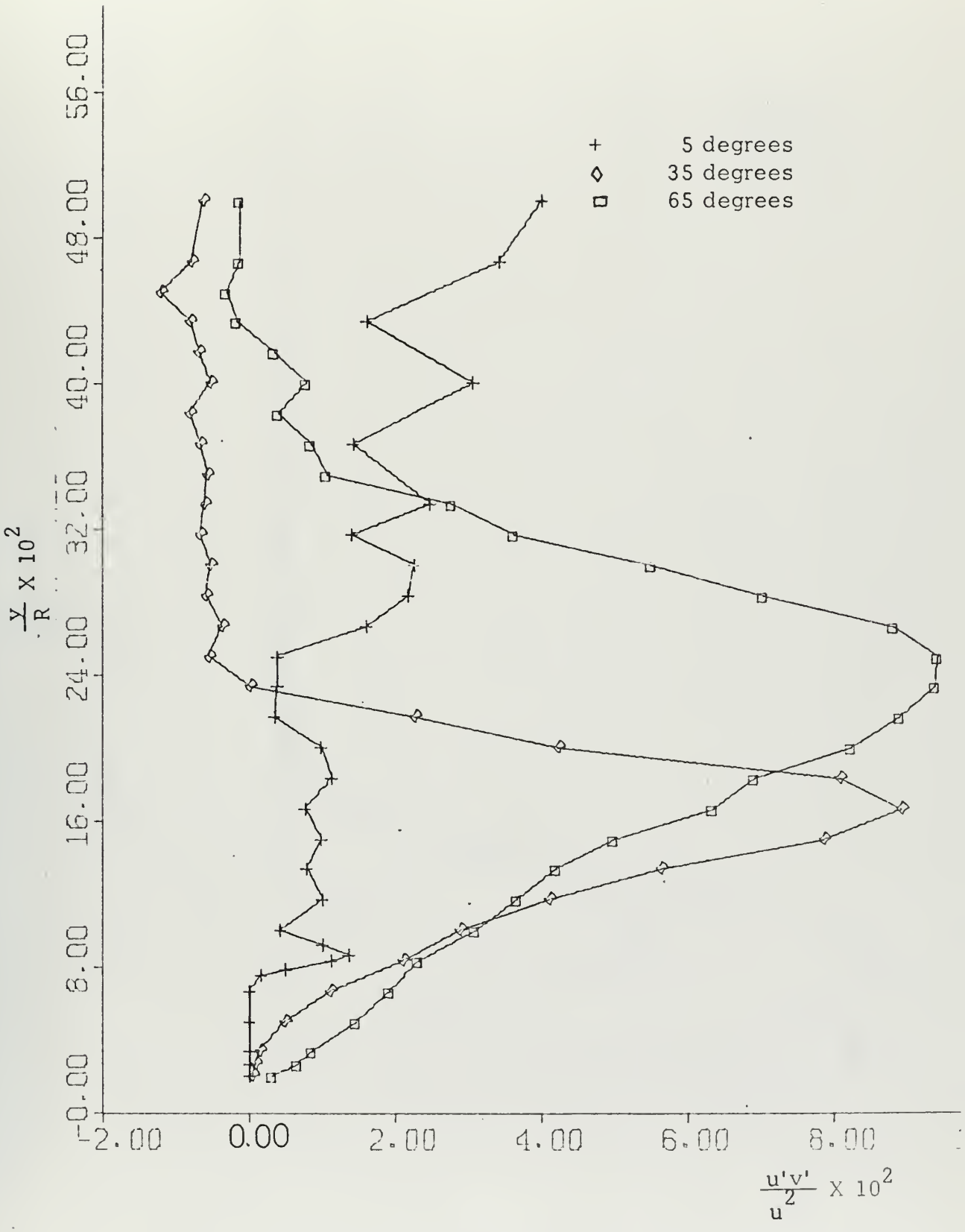

FIG. 20. Distribution of Local Turbulent Shear Stress, $Re_w = 21040$

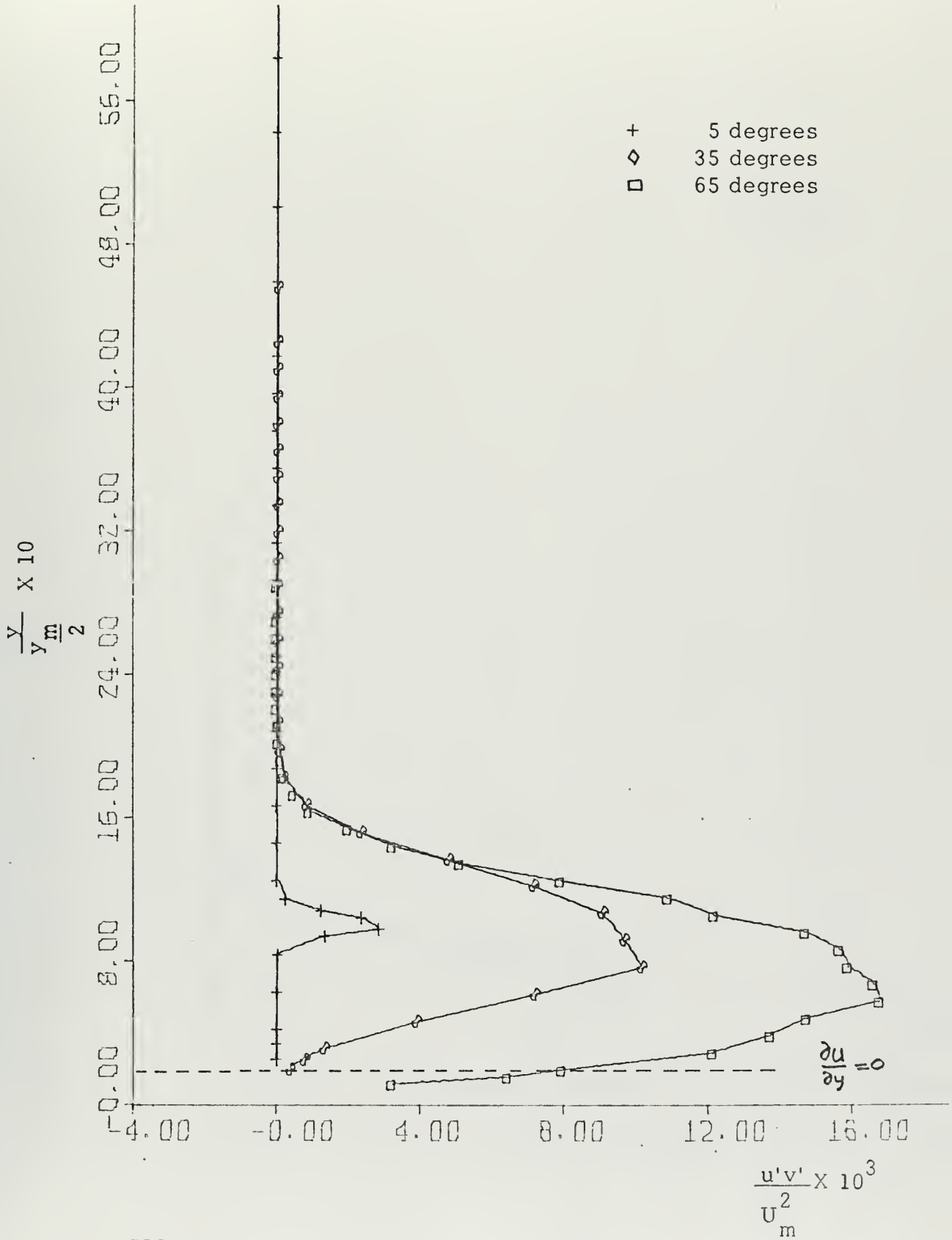

FIG. 21. Distribution of Turbulent Shear Stress, $Re_w = 21040$

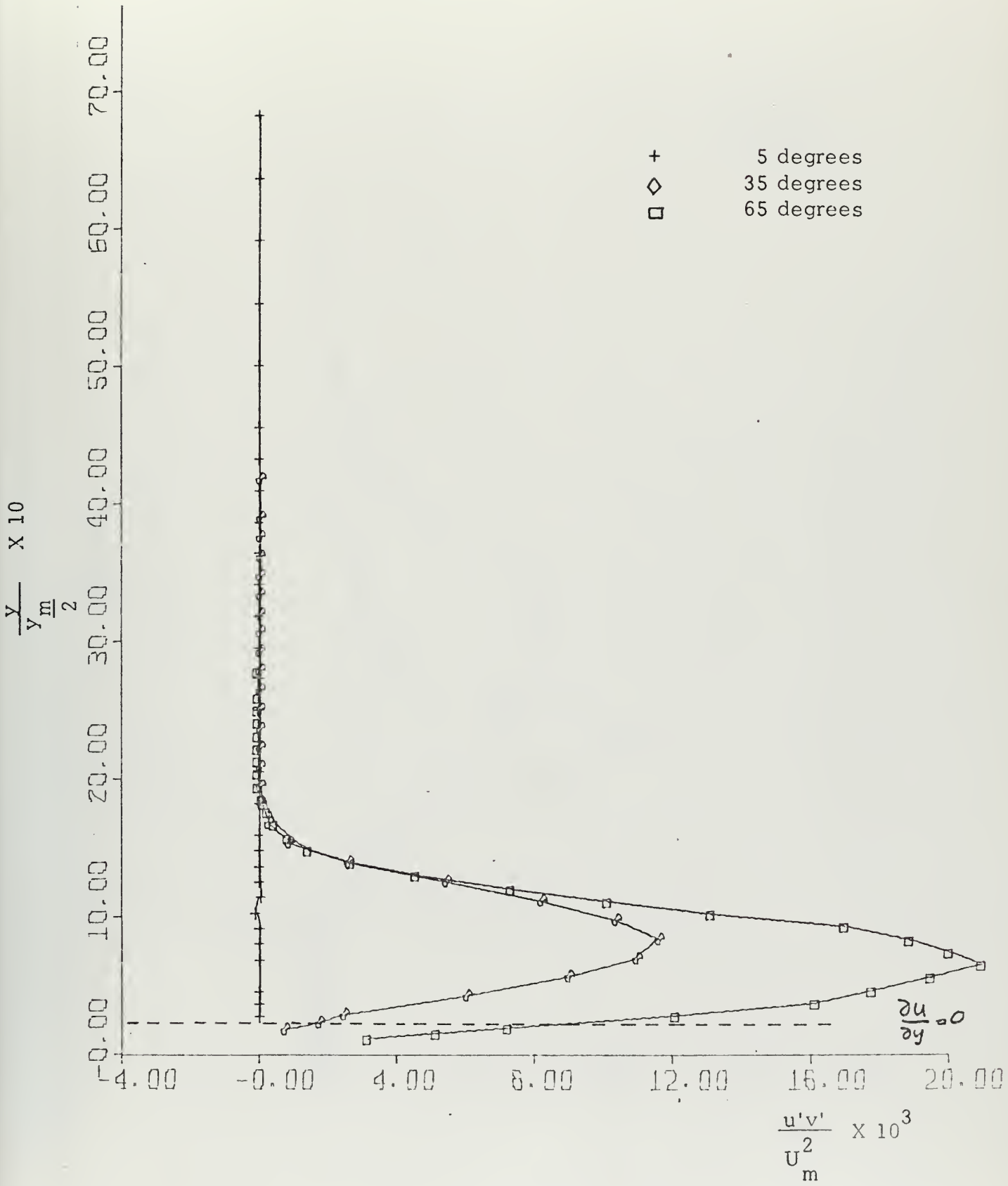

FIG. 22. Distribution of Turbulent Shear Stress, Re_w = 9340

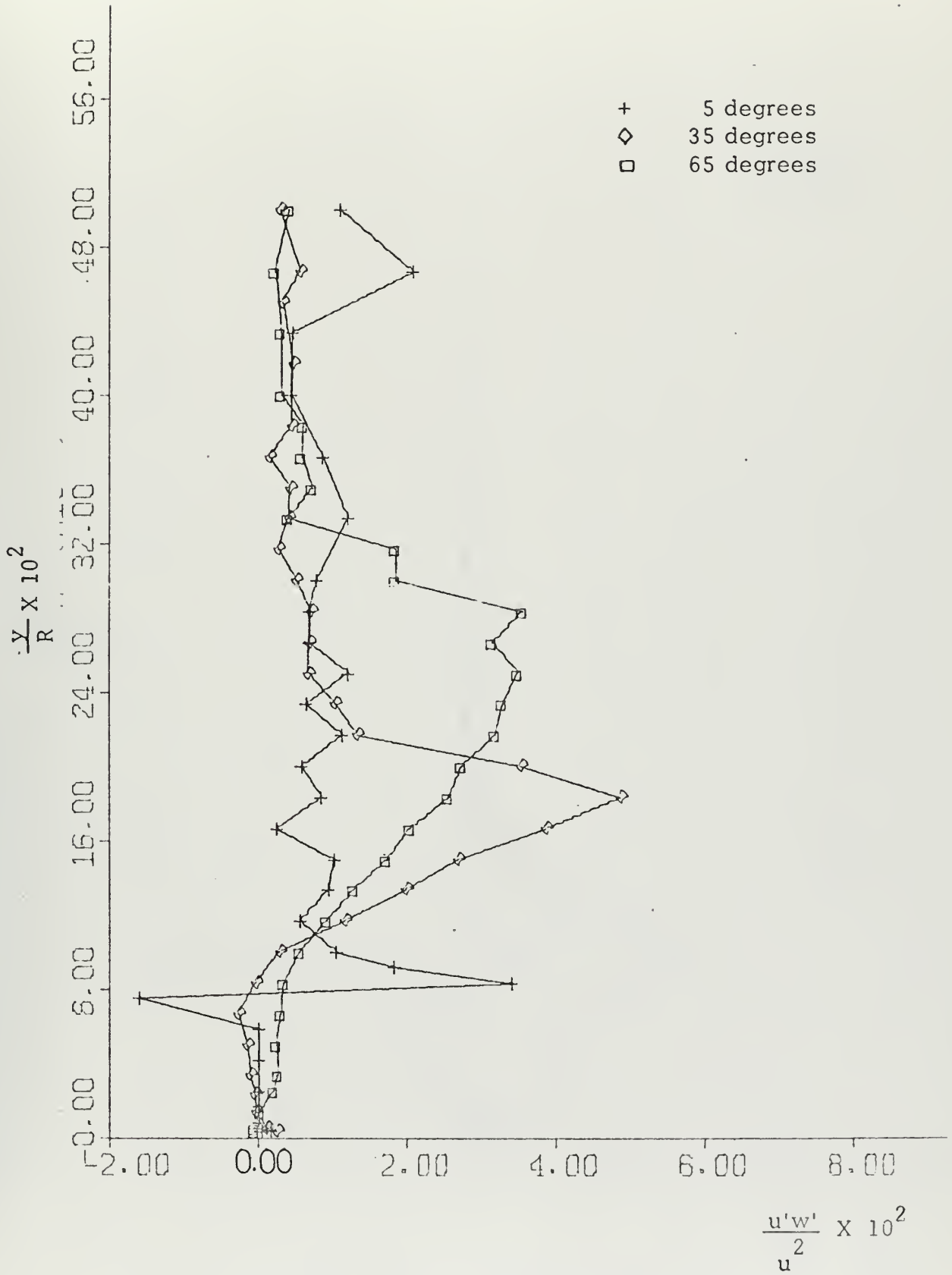

FIG. 23. Distribution of Local Turbulent Shear Stress, $Re_w = 21040$

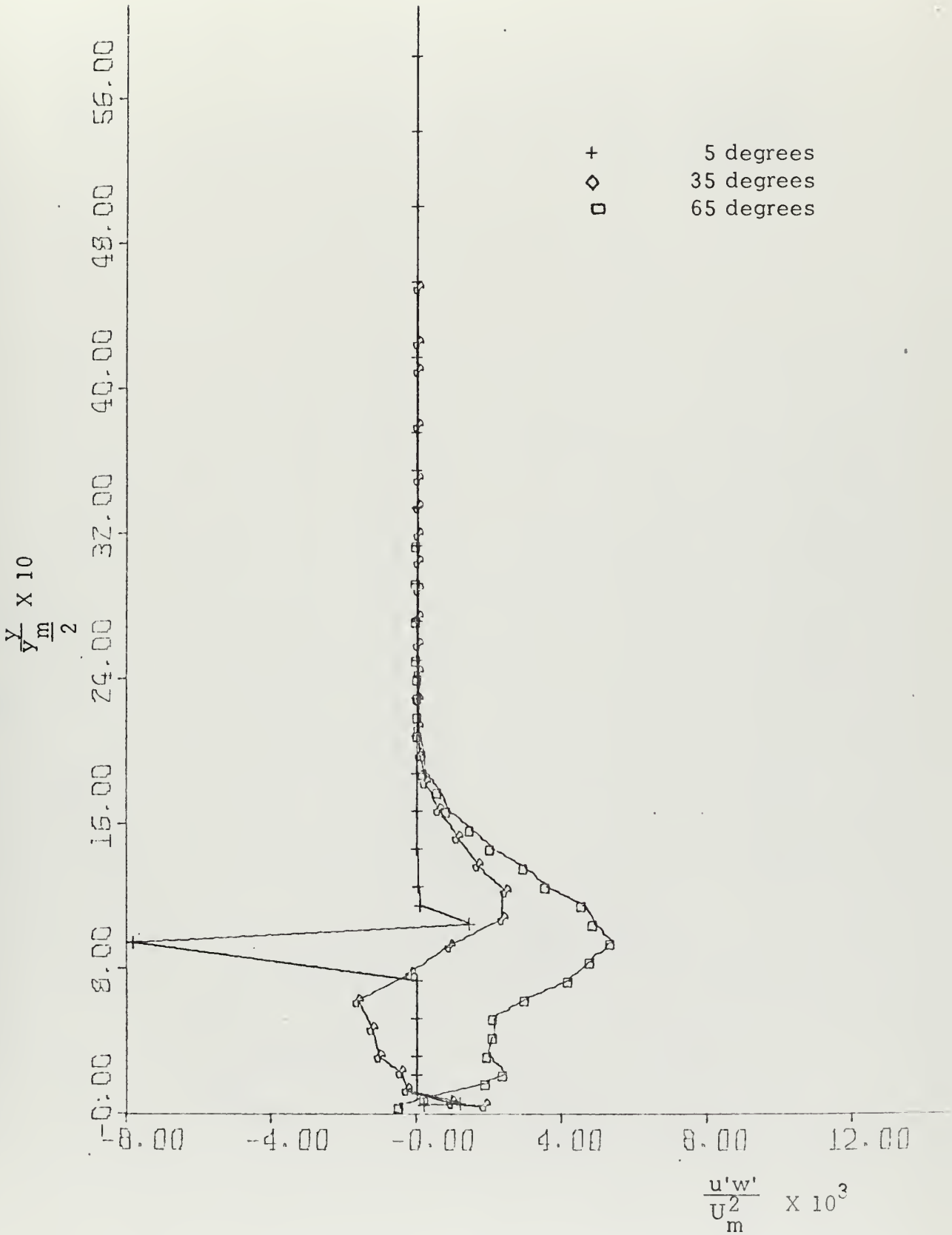

FIG. 24. Distribution of Turbulent Shear Stress, Re_w = 21040

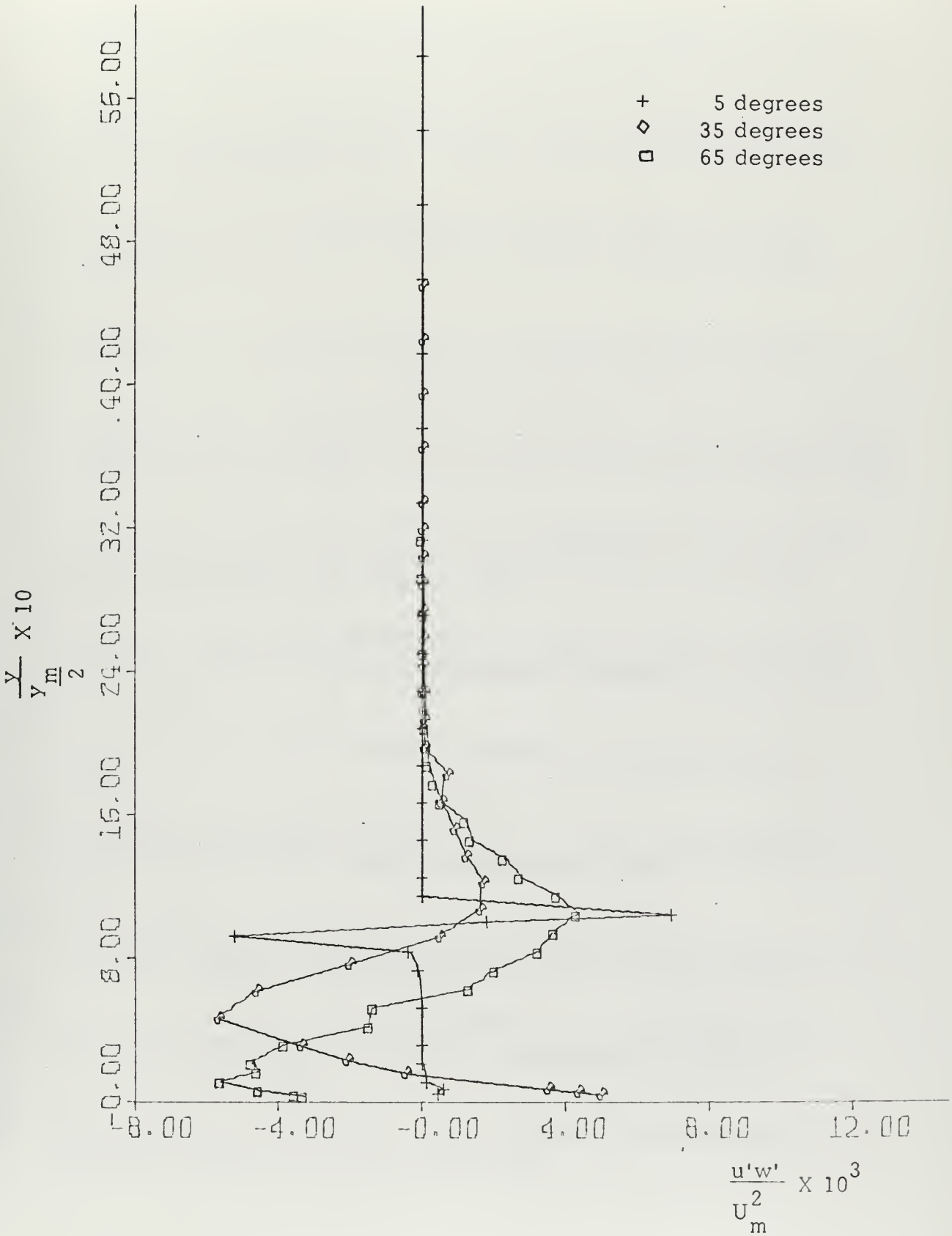

FIG. 25. Distribution of Turbulent Shear Stress, $Re_w = 9340$

LIST OF REFERENCES

1. Kesler, K., Turbulent Jet Attachment to Convex Walls, M.S. Thesis, Naval Postgraduate School, Monterey, June 1968.

2. Johnson, L. D., Experimental Investigation of Turbulent Jet Attachment to a Convex Wall, M.S. Thesis, Naval Postgraduate School, Monterey, September 1968.

3. Richardson, D. C., Jet Attachment to Coanda Walls in Bistable Amplifiers, M.S. Thesis, Naval Postgraduate School, Monterey, April 1969.

4. Sawyer, R. A., "The Flow due to a Two-Dimensional Jet Issuing Parallel to a Flat Plate," Journal of Fluid Mechanics, December 1960.

5. Newman, B. G., "The Deflection of Plane Jets by Adjacent Boundaries--Coanda Effect," Boundary Layer and Flow Control--Its Principles and Applications, edited by G. V. Lachmann, Vol. 1, Pergamon Press 1961.

6. Fekete, G. I., "Coanda Flow of a Two-Dimensional Wall Jet on the Outside of a Circular Cylinder," McGill University Mechanical Engineering Dept., Report 63-11, 1963.

7. Guitton, D. E., "Two Dimensional Turbulent Wall Jets over Curved Surfaces," McGill University Mechanical Engineering Dept., Report 64-7, 1964.

8. Glauert, M. D., "The Wall Jet," Journal of Fluid Mechanics, Vol. 1, 1956.

9. Wyganski, I. J., and Champagne, F. H., "The Laminar Wall-Jet over a Curved Surface," Journal of Fluid Mechanics, Vol. 31, Part 3, 1968.

10. Schwarz, W. H. and Cosart, W. P., "The Two Dimensional Turbulent Wall-Jet," Journal of Fluid Mechanics, Vol. 10, Part 4, 1961.

11. Giles, J. A., Hays, A. P., and Sawyer, R. A., "Turbulent Wall Jets on Logarithmic Spiral Surfaces," Aeronautical Quarterly, Vol. XVII, August 1966.

12. Margolis, D. P. and Lumley, J. L., "Curved Turbulent Mixing Layer," Physics of Fluids, Vol. 8, No. 10, 1965.

13. Schlichting, H., Boundary Layer Theory, IVth Ed., McGraw Hill, 1960.

14. Sawyer, R. A., "Two Dimensional Reattaching Jet Flows Including the Effects of Curvature on Entrainment," Journal of Fluid Mechanics, December 1963.

15. Poreh, M., Tsuei, Y. G., Cermak, J. E., "Investigation of a Turbulent Radial Wall Jet," Journal of Applied Mechanics, June 1967.

16. Eskinazi, S. and Yeh, J., Journal of Aerospace Science, Vol. 28, No. 23 (1956).

INITIAL DISTRIBUTION LIST

		No. Copies
1.	Defense Documentation Center Cameron Station Alexandria, Virginia 22314	2
2.	Library, Code 0202 Naval Postgraduate School Monterey, California 93940	2
3.	Asst Professor T. Houlihan, Code 59Hm Department of Mechanical Engineering Naval Postgraduate School Monterey, California 93940	1
4.	LCDR K. R. L. Perera c/o Royal Ceylon Navy Headquarters P. O. Box 593 Colombo, Ceylon	1

DOCUMENT CONTROL DATA - R & D

(Security classification of title, body of abstract and indexing annotation must be entered when the overall report is classified)

1. ORIGINATING ACTIVITY (Corporate author)
Naval Postgraduate School
Monterey, California 93940

2a. REPORT SECURITY CLASSIFICATION
Unclassified

2b. GROUP

3. REPORT TITLE
Curved Wall Boundary Layer Flow

4. DESCRIPTIVE NOTES (Type of report and inclusive dates)
Master's Thesis; June 1971

5. AUTHOR(S) (First name, middle initial, last name)
K. R. L. Perera

6. REPORT DATE
June 1971

7a. TOTAL NO. OF PAGES
56

7b. NO. OF REFS
16

8a. CONTRACT OR GRANT NO.

b. PROJECT NO.

c.

d.

9a. ORIGINATOR'S REPORT NUMBER(S)

9b. OTHER REPORT NO(S) (Any other numbers that may be assigned this report)

10. DISTRIBUTION STATEMENT
Approved for public release; distribution unlimited.

11. SUPPLEMENTARY NOTES

12. SPONSORING MILITARY ACTIVITY
Naval Postgraduate School
Monterey, California 93940

13. ABSTRACT

Mean velocities, turbulence intensities, and Reynolds stresses were measured in a circular convex wall jet. The entire mean velocity profile for angular position 0 35 degrees was determined to be similar. The turbulent flow field was nowhere self preserving and thus the total flow was not similar. Strikingly different jet growth rates were evidenced between the inlet (0 35 degrees) transition region and the fully developed flow regions (0 35 degrees). The overall level of turbulence was found to be higher for a convex wall jet flow in comparison to a concave wall jet flow. However, maximum turbulence inteisities occurred closer to the wall for increasing distance along the surface indicating the stabilizing effect of the convex wall. The turbulent shear stress $\overline{u'v'}$ was dominant in comparison with $\overline{u'w'}$ and did not vanish where the mean velocity gradient became zero. Hence for further analyses of turbulent convex wall jet flow the classical eddy viscosity models which neglect the effects of curvature cannot be incorporated.

KEY WORDS	LINK A		LINK B		LINK C	
	ROLE	WT	ROLE	WT	ROLE	WT
Convex surface						
Curved wall jet						
Turbulent flow						
Fluidics						

18 APR 72 20483

Thesis 128396
P3353 Perera
c.1 Curved wall boundary
layer flow.

18 APR 72 20483

Th
P3
c.1

Thesis 128396
P3353 Perera
c.1 Curved wall boundary
layer flow.

thesP3353
Curved wall boundary layer flow.
3 2768 001 97970 1
DUDLEY KNOX LIBRARY